SANDIA REPORT SAND86—1133 • Unlimited Release • UC—92a
Printed June 1986

High-Energy Gas Fracturing in Cased and Perforated Wellbores

J. F. Cuderman

Prepared by
Sandia National Laboratories
Albuquerque, New Mexico 87185 and Livermore, California 94550
for the United States Department of Energy
under Contract DE-AC04-76DP00789

DISCLAIMER

Issued by Sandia National Laboratories, operated for the United States Department of Energy by Sandia Corporation.

Printed in the United States of America
Available from
National Technical Information Service
U.S. Department of Commerce
5285 Port Royal Road
Springfield, VA 22161

NTIS price codes
Printed copy: A03
Microfiche copy: A01

SAND86-1133
Unlimited Distribution
Printed June 1986

UC Category 92a

HIGH-ENERGY GAS FRACTURING IN CASED AND PERFORATED WELLBORES

J. F. Cuderman

SAND--86-1133

DE86 013068

ABSTRACT

A propellant-based technology, High-Energy Gas Fracturing (HEGF), has been applied to fracturing through perforations in cased boreholes. HEGF is a tailored-pulse fracturing technique originally developed by Sandia National Laboratories for application in uncased, liquid-free gas wells in Appalachian Devonian shales. Because most oil and gas wells are liquid filled as well as cased and perforated, the potential impact of present research is significantly broader. A number of commercial tailored-pulse fracturing services, using a variety of explosives or propellants, are currently available. Present research provides valuable insight into phenomena that occur in those stimulations.

The use of propellants that deflagrate or burn rather than detonate, as do high-order explosives, permits controlled buildup of pressure in the wellbore. The key to successful stimulation in cased and perforated wellbores is to control the pressure buildup of the combustion gases to maximize fracturing without destroying the casing. Eight experiments using cased and perforated wellbore were conducted in a tunnel complex at the Department of Energy's Nevada Test Site, which provides a realistic in situ stress environment (4-10 MPa [600-1500 psi]) and provides access for mineback to directly observe fracturing obtained. Primary variables in the experiments include propellant burn rate and amount of propellant used, presence or absence of liquid in the wellbore, in situ stress orientation, and perforation diameter, density, and phasing. In general, the presence of liquid in the borehole results in a much faster pressure risetime and a lower peak pressure for the same propellant charge. Fracture surfaces proceed outward along lines of perforations as determined by phasing, then gradually turn toward the hydraulic fracture direction.

CONTENTS

ILLUSTRATIONS

ILLUSTRATIONS (Continued)

TABLES

HIGH-ENERGY GAS FRACTURING IN CASED AND PERFORATED BOREHOLES

1. INTRODUCTION

High-Energy Gas Fracturing (HEGF) is a propellant-based technology developed to enhance production in natural-gas wells. The basic concept behind HEGF is that because propellants are manufactured in a wide range of sizes and burn rates, careful selection of type and quantity of propellant can produce borehole pressurization rates that create multiple, radial fractures emanating from the wellbore.

Propellant-based fracturing is advantageous over conventionally used explosive, foam, and hydraulic fracturing because propellant-based fracturing provides control over the type of fracturing produced. Very fast propellants (<0.1 ms pressure risetime) produce results similar to those from explosives, which detonate; both produce a crushed zone about the wellbore that can decrease transmissivity in the rock immediately surrounding the wellbore. Slow propellants (>1 ms pressure risetime) produce results similar to those of foam and hydraulic fracturing; only a single hydraulic-type fracture is propagated. Because hydraulic-type fractures often parallel existing natural fractures, additional natural fractures are not connected to the wellbore. When propellants with intermediate burn rates (0.1 to 1 ms pressure risetimes) are used, however, four to eight radial fractures can be produced. The radial fracture pattern tends to intersect natural fractures that otherwise would not communicate with the wellbore, thereby enhancing the potential of increasing production.

The initial research and development for HEGF focused on producing a methodology for specifying propellants to achieve the desired pressure pulse and fracture pattern in liquid-free, uncased boreholes.

Work proceeded in three areas: (1) hardware development, (2) field tests, and (3) modeling activities (Cuderman, 1984a; Cuderman and Northrop, 1984; Cuderman, 1984b; Cuderman, 1984c). Hardware development solved problems such as how best to contain and ignite the propellant, how best to isolate the interval of borehole to be pressurized, and how to instrument the test so that the pressurization could be recorded. Field tests included several series of in situ experiments to determine pressure pulse and fracture behavior as a function of borehole diameter and propellant mixture. Most tests were conducted in G-Tunnel at the Department of Energy's Nevada Test Site (NTS), a location that provided a realistic geologic environment and where the fracture patterns were directly observable by mining back to uncover the test bed. Tests in Devonian shale at Rowan County, Kentucky, and Meigs County, Ohio, proved the technology was equally applicable to producing gas wells. Models developed enable predictions of (1) pressure risetimes and propellant mixtures required for multiple fracturing, (2) stress and acceleration in the formation as a result of a given pressure pulse, and (3) fracture type, length, and orientation.

The background work formed the basis for the technology of propellant-based fracturing. Data from more than 30 field tests demonstrated that for liquid-free, uncased boreholes, (1) the pressure risetime, t_m, is the most critical factor in determining the type of fracturing obtained, (2) the pressure risetime can be controlled by properly mixing propellants, and (3) the principal far-field in situ stresses generally control fracture orientation and, to a certain extent, fracture length.

Figure 1 is a typical pressure pulse obtained during multiple fracturing in uncased, liquid-free wellbores. An initial pressure rise is normally observed, after which the pressure drops and then increases again until the propellant burn is complete. The pressure drop after the initial rise is interpreted as being due to the increase in free volume accompanying fracture initiation. The time between initial pressure rise and the initial peak is the pressure risetime.

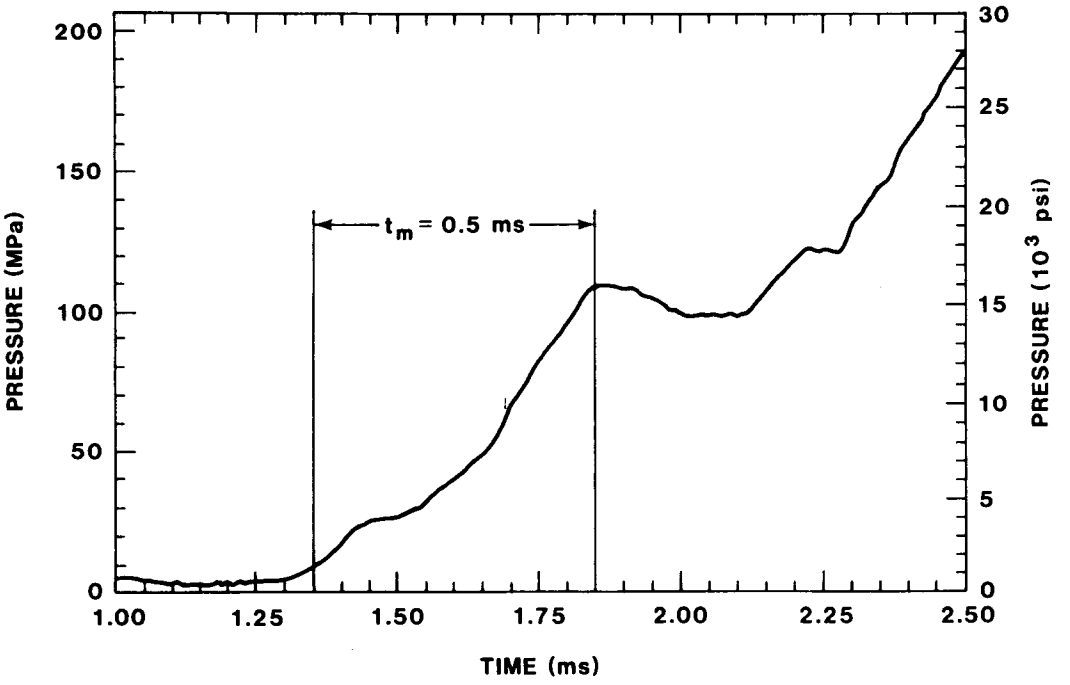

Figure 1. Plot of Characteristic Pressure History

The multiple-fracture regime is defined in terms of pressure risetime, t_m, by

$$\frac{\pi D}{2C_R} < t_m < \frac{8\pi D}{C_R} \qquad (1)$$

where C_R is the Raleigh surface-wave velocity and D is the borehole diameter. The equation holds for any rock type whose Poisson's ratio is in the vicinity of 0.3 (Cuderman, 1984a). The term at the left in Equation 1 is a derived result (Cuderman, 1984a) that represents the boundary between the multiple- and explosive-fracture regimes. The term at the right represents the boundary between the hydraulic- and multiple-fracture regimes. This term was derived by assuming the same scaling relationship used for the multiple-explosive boundary, but with a different multiplying factor. The multiplying factor was determined empirically.

Figure 2 shows the explosive-, multiple-, and hydraulic-fracture regimes defined by Equation 1. Note that smaller-diameter boreholes require faster risetimes for equivalent fracturing. Test results indicate that Equation 1 is equally applicable to ash-fall tuff and Devonian shale (Cuderman, 1984a; Cuderman and Northrop, 1984; Cuderman, 1984c).

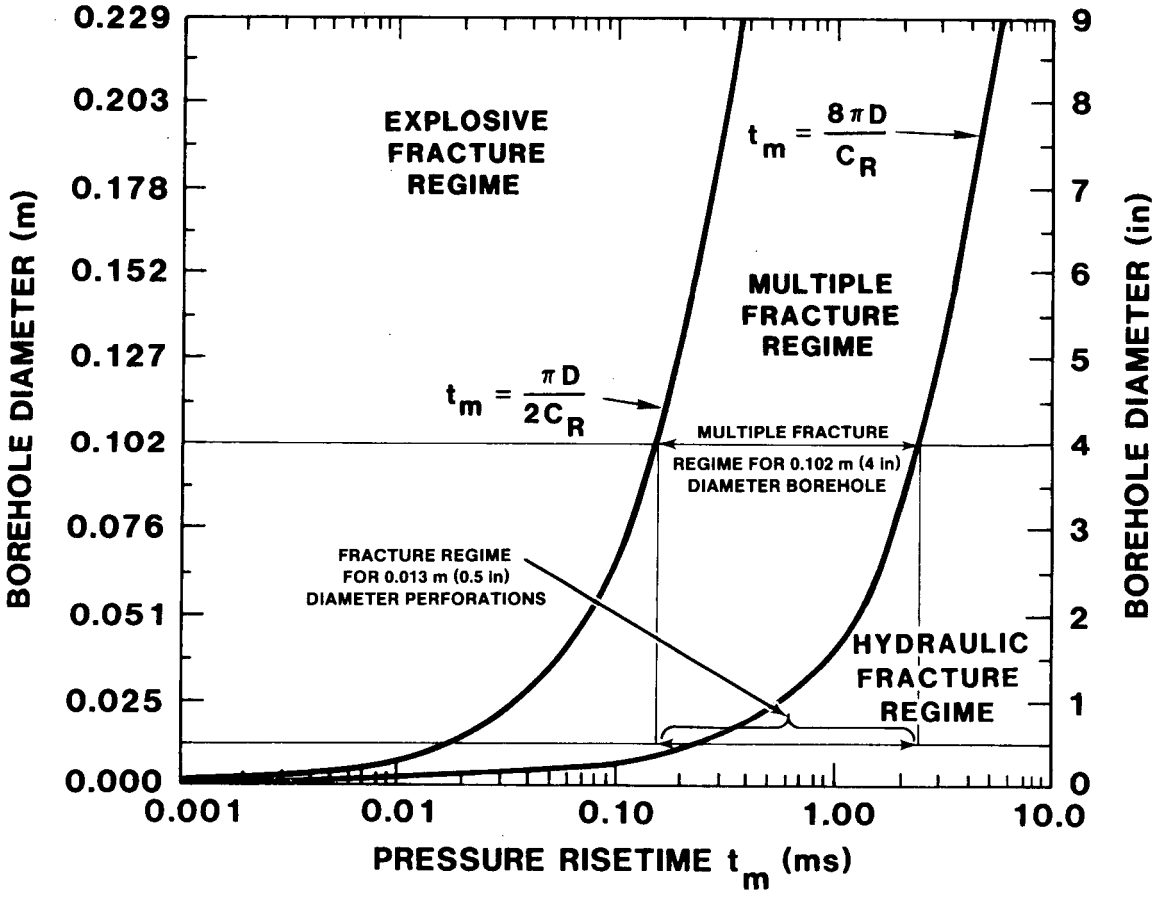

Figure 2. Risetime-Specification Plot

Figure 3 is a schematic of an optimum multiple-fracture pattern from a liquid-free borehole experiment. In this example, the borehole parallels one of the far-field principal in situ stress directions, with the maximum and minimum principal in situ stresses in the plane normal to the borehole axis designated as σ_1 and σ_2, respectively. As shown in Figure 3, the largest fracture produced is normal to the minimum principal in situ stress (σ_2), with another major fracture

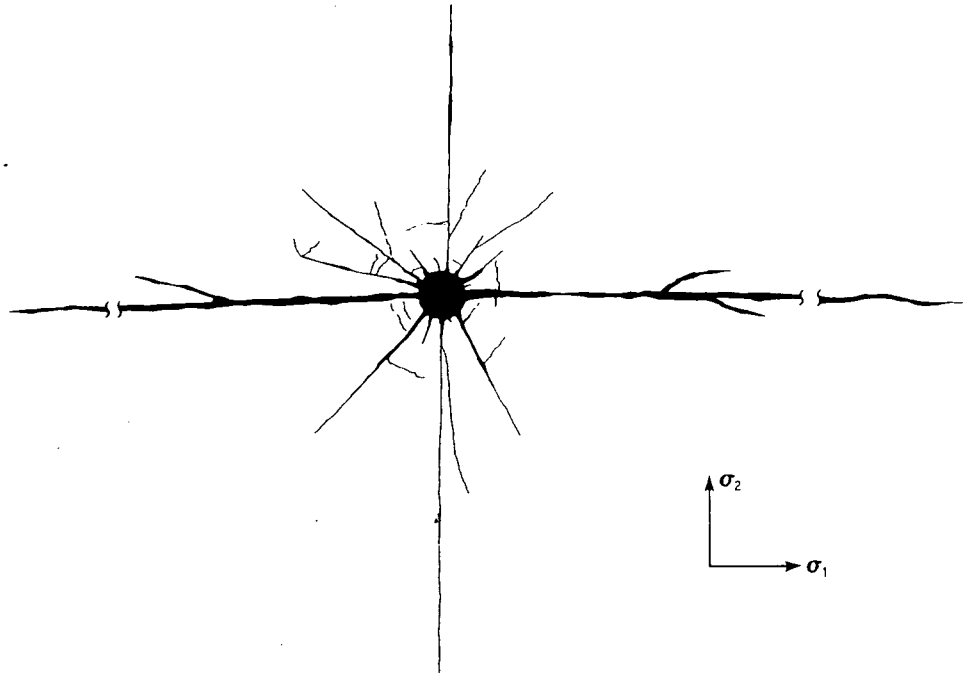

Figure 3. Schematic of Multiple-Fracture Pattern

oriented normal to the maximum in situ stress (σ_1). Semimajor fractures at 45° to the major fractures correspond to principal shear planes. The principal stress parallel to the borehole does not influence fracturing behavior under these dynamic conditions.

The fracture pattern depicted in Figure 3 is produced when pressure risetimes are in that portion of the multiple-fracture regime closest to the boundary with the explosive-fracture regime. For pressure risetimes in the hydraulic-fracture regime, only a single fracture normal to the minimum principal in situ stress (σ_2) occurs. For risetimes in the multiple-fracture regime, but near the hydraulic boundary, additional fractures appear normal to the maximum principal in situ stress (σ_1). For risetimes in the center of the multiple-fracture region, fractures also appear along shear planes in each of the four quadrants bounded by principal stress planes. Pressure risetimes near the center of multiple-fracture regime produce shear plane fractures oriented about 30° relative to σ_1, while pressure risetimes that approach the boundary between the multiple- and

explosive-fracture regimes produce shear plane fractures closer to 45°. The 30° case coincides with brittle fracture behavior, while the 45° case characterizes near-ductile failure.

Because pressure risetime is so critical to optimizing fracturing, formulation of a propellant mixture that produces the desired risetime is essential. Early development tests showed that standard ballistics calculations do not predict with sufficient accuracy the pressure risetimes for a given borehole diameter and propellant type. Risetimes from field tests are always faster than predicted by the ballistics calculations, probably because the propellant canisters used contain a rapid-ignition primer (RIP) that introduces an instantaneous burst of flame and pressure; standard ballistics calculations assume a gradual pressure buildup. Thus, empirical data replaced the ballistics calculations. An equation was derived for formulating the propellant mixture that produces the desired pressure risetime. The equation is

$$f_A = \frac{\log\left(t_B/t_m\right)}{\log\left(t_B/t_m\right) + 2\,\log\left(t_m/t_A\right)} \qquad (2)$$

where f_A is the required fraction by weight of the faster-burning propellant for the propellant mix, t_A is the risetime of pure faster-burning propellant, t_B is the risetime of pure slower-burning propellant, and t_m is the desired risetime. Note that values for t_A and t_B must be obtained using the same volume of propellant and volume pressurized (borehole diameter times length of test interval) as that to be used in the stimulation for which the propellant mixture is being formulated. Also note that peak pressure is not a required parameter for optimizing fracturing.

Application of HEGF to Cased and Perforated Boreholes

Because most gas wells are cased and perforated, a question repeatedly asked by the petroleum industry was whether or not the HEGF technology is applicable to cased and fluid-filled boreholes. To

answer this question, three series of four experiments each were designed and fielded. Two experiments in Test Series #1 and two experiments in Test Series #2 used uncased, fluid-filled boreholes. Results from these experiments were discussed previously (Cuderman et al, 1986; Cuderman, 1986a). Results from the remaining eight experiments are discussed in this report.

The objectives of the research were to determine (1) whether one could obtain multiple fracturing through perforations, (2) the extent of such fractures, (3) pressure rates required for optimizing fracturing, (4) attendant casing damage, and (5) the effect of fluid on borehole pressurization.

2. DESIGN AND INSTALLATION OF EXPERIMENTS USING CASED AND PERFORATED WELLBORES

Important Variables in Fracturing Through Perforations

In HEGF fracturing of uncased wellbores, the pressure risetime as a function of borehole diameter and rock type proved to be the critical variable defining the type of fracturing obtained. The addition of perforated casing provides additional constraints. Factors controlling fracturing through cased and perforated boreholes include

(1) Perforation diameter
(2) Number of perforations per unit length of casing (perforation density)
(3) Propellant burn rate
(4) Propellant charge size
(5) Perforation orientation
(6) Presence or absence of liquid in the borehole

The number and diameter of perforations determine gas flow out of the casing during propellant burn. If this exit area is insufficient, the casing acts as a gas bottle until either completion of the burn or rupture of the casing. Because casing splits must be avoided, either the number and diameter of perforations must be increased, the quantity of propellant must be reduced, or the propellant burn rate must be sufficiently slow that the propellant gas has ample time to exit the wellbore.

Effect of Perforation Diameter and Density on Wellbore Pressurization

An estimate of maximum mass of the gas exiting through perforations can be made using the equation for choked flow:

$$\frac{dm}{dt} = (\text{constant})\ PNd^2 \qquad (3)$$

where dm/dt is the mass flow per unit time, P is the pressure, N is the number of perforations, and d is perforation diameter.

The rate of pressure loss at a given pressure can be derived from the gas-law equation:

$$PV = nkT \tag{4}$$

where P is the pressure, V is volume of the test zone, n is the number of molecules of gas, k is Boltzman's constant, and T is absolute temperature.

Differentiating Equation 4 yields:

$$\frac{dP}{dt} = \frac{kT}{V}\frac{dn}{dt} \tag{5}$$

Given that $n = A_o \frac{m}{M}$

where m is mass of gas, M is molecular weight, and A_o is Avogadro's constant, then

$$\frac{dP}{dt} = \frac{A_o kT}{MV}\frac{dm}{dt} \tag{6}$$

Substituting Equation 3 into Equation 6 results in

$$\frac{dP}{dt} = (\text{constant})\ \frac{PNd^2A_o kT}{MV} \tag{7}$$

Equation 7 shows that for a given pressure and temperature from a given propellant, the pressure decrease per unit time through perforations is proportional to the number of perforations (N) and to the square of the perforation diameter (d). As a result, the pressure

within the casing is more effectively controlled by varying perforation size than by increasing the number of perforations.

Effect of Perforation Orientation and Phasing on Fracturing

Experiments in fluid-free uncased boreholes demonstrated that the type of fracturing obtained is governed by the pressure risetime in the borehole (Cuderman, 1984a; Cuderman and Northrop, 1984). Recall that for multiple fracturing, the risetime must be in the range

$$\frac{\pi D}{2C_R} < t_m < \frac{8\pi D}{C_R} \qquad (1)$$

Longer risetimes result in hydraulic fracturing, and shorter risetimes result in explosive fracturing or wellbore crushing. For cased and perforated boreholes, pressure risetimes corresponding to crushing in uncased wellbores logically can be expected to deform or split casing. Figure 2, the plot of Equation 1, shows that pressure risetimes required to produce multiple fracturing in nominal-sized boreholes (0.1 m [4 in] or larger), however, will not produce multiple fractures in the perforation channels (diameters typically 0.015 m [0.6 in] or less), which for this simplified model can be regarded as miniature boreholes. Only a hydraulic-type fracture can be obtained in each perforation.

Orientation of the hydraulic fracture can be predicted by analyzing an example of a cased, perforated wellbore oriented along the maximum principal stress (σ_1) in a formation (Figure 4). Previous research in uncased wellbores showed that fracture geometry is governed by the principal far-field in situ stresses normal to the wellbore and that the principal in situ stress parallel to the wellbore does not appear to affect fracturing (Cuderman, 1984a; Cuderman and Northrop, 1984). Consider the situation where a line of perforations is oriented at some angle θ to the minimum in situ stress (Figure 4a). This is the geometry used in all experiments in cased and perforated wellbores at NTS to date and is typical of gas and oil wells.

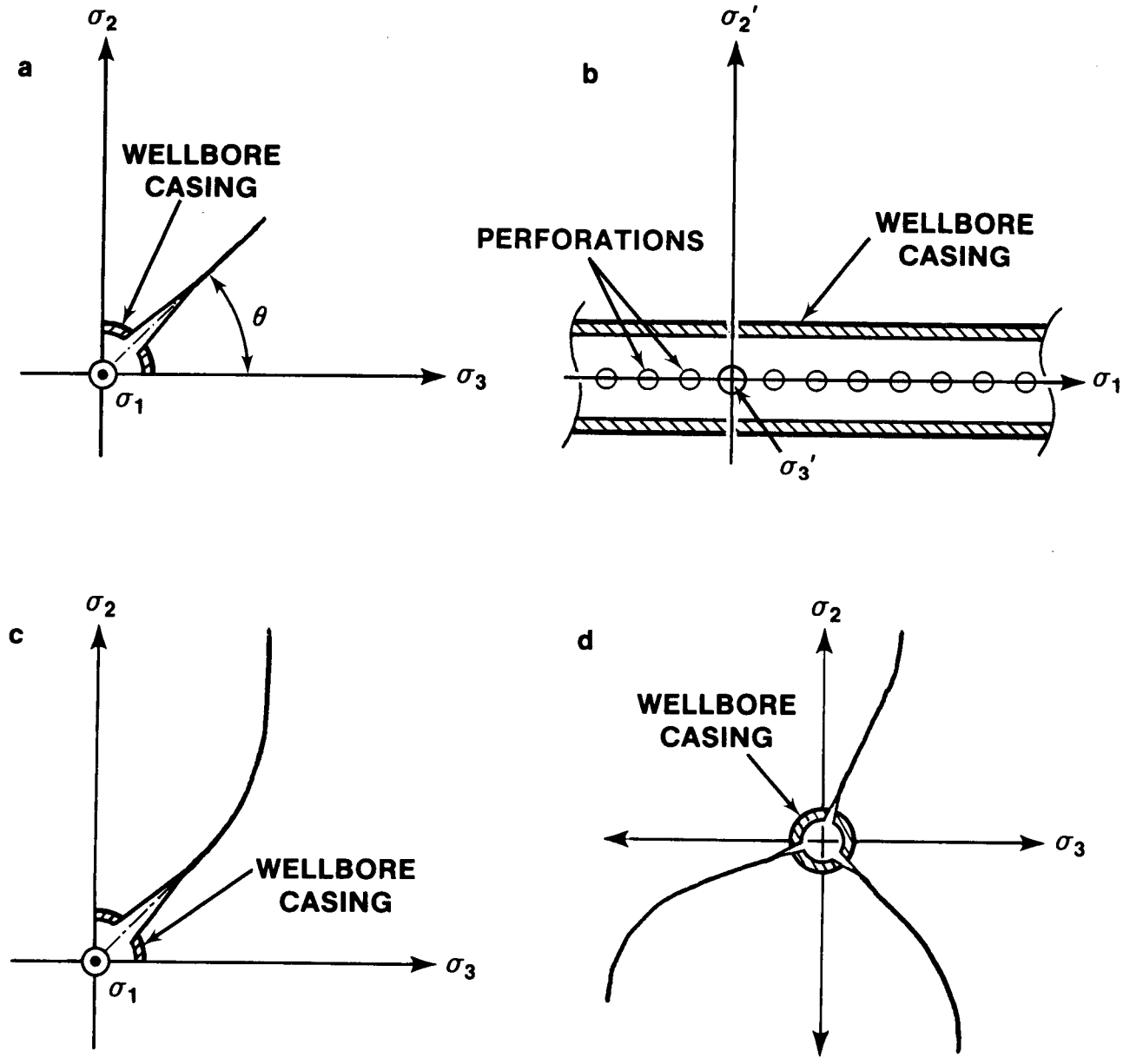

Figure 4. Schematic of Perforation Orientation and Predicted Fracture Pattern

Assuming that each perforation channel acts as a miniature borehole, the principal far-field in situ stress components normal to the perforation are

$$\sigma_1' = \sigma_1 \tag{8}$$

$$\sigma_2' = \sigma_2 \cos^2\theta + \sigma_3 \sin^2\theta \tag{9}$$

The component parallel to the perforation is

$$\sigma_3' = (\sigma_2 - \sigma_3) \sin\theta \cos\theta \tag{10}$$

These principal stress components are shown relative to the perforation in Figure 4b where the perforation channel is oriented into the plane of the paper along the σ_3' direction. Because only hydraulic-type fracturing is expected in the perforation channels, and σ_2' is always less than σ_1, the fracture obtained in the perforations will be perpendicular to σ_2' in the plane of σ_1 and σ_3'. Fractures from individual perforations are therefore aligned, so that they can combine to form a single fracture plane going through all of the perforations. The predicted fracture is depicted in Figure 4c.

This fracture surface should first proceed in the general perforation direction, and then gradually turn toward the far-field hydraulic fracture direction normal to the minimum in situ stress (σ_2). If the perforations are oriented along σ_2 or σ_3, such turning may be minimal and longer fractures may be produced. Figure 4d shows the fracture geometry expected for a 120°-phase, randomly oriented perforation geometry.

It is understood that the actual stresses in the vicinity of the wellbore and its perforations are more complex than depicted in the model. However, a more exact analysis using actual stresses near a borehole (Jaeger and Cook, 1975) yields the same predictions. This is

because the direction of maximum and minimum stresses about the borehole matches those of the principal far-field in situ stresses, and the relative order of their magnitudes, $\sigma_1 > \sigma_2 > \sigma_3$, remains the same.

All of the data from tailored-pulse fracturing through perforations, to date, with σ_1 parallel to the wellbore, match predicted results from this model (Cuderman, 1986b). However, additional experiments are needed to determine whether the simplified model is generally valid for predicting fracture directions in perforation channels or whether near-field stress perturbations need to be included. An important test would be one in which the minimum principal stress is parallel to the wellbore axis.

Test-Bed Preparation

Eight experiments, designated A through H, that involved cased, perforated wellbores were conducted in the end face of drifts in the G-Tunnel complex at NTS. Test Series #1 and #2 were located in the MAC drift, where principal far-field in situ stresses are σ_1 = 10.3 MPA (1490 psi), σ_2 = 8.6 MPa (1250 psi), and σ_3 = 5.4 MPa (780 psi). Test Series #3 was moved to the PTE 2 drift, where principal far-field in situ stresses are σ_1 = 6.9 MPa (1000 psi), σ_2 = 5.9 MPa (850 psi), and σ_3 = 3.8 MPa (550 psi). In all eight experiments, the boreholes were aligned parallel to the maximum principal in situ stress direction because this typifies conditions in an oil or gas well where the borehole generally parallels the maximum principal in situ stress direction.

Each test series consisted of four experiments arranged in a 2-by-2 array (Figure 5). In Test Series #1 and #2, the two experiments on the right side of the tunnel face were not cased, and results were discussed elsewhere (Cuderman et al, 1986). Note that tuff lithology is not uniform in the two test beds. In Test Series #3, however, the test bed was almost entirely red ash-fall tuff. A listing of the properties of the two predominate tuff units in the three tests is provided in Table 1.

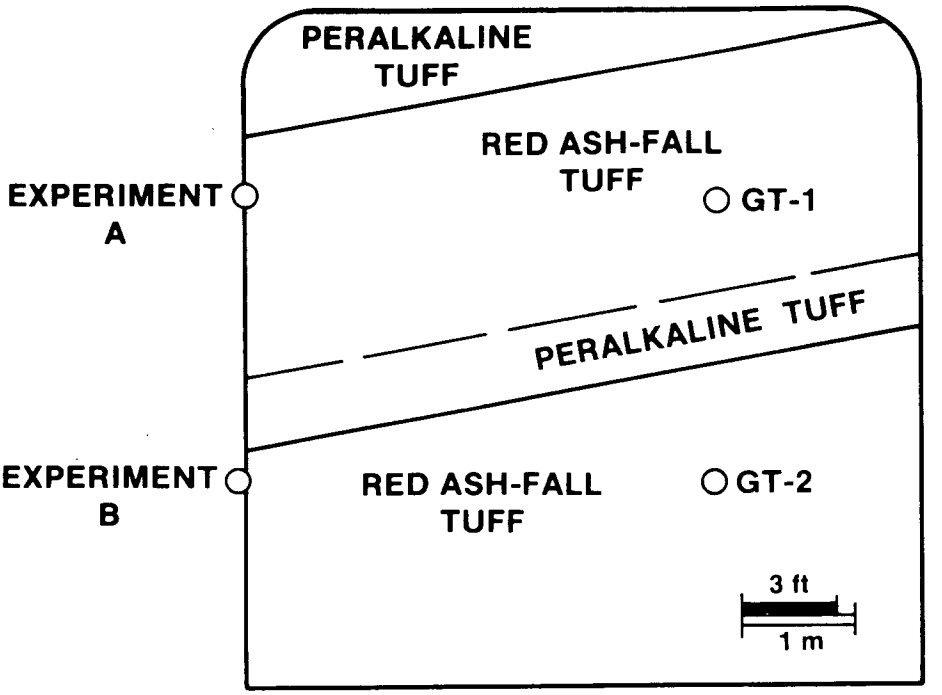

TEST SERIES #1

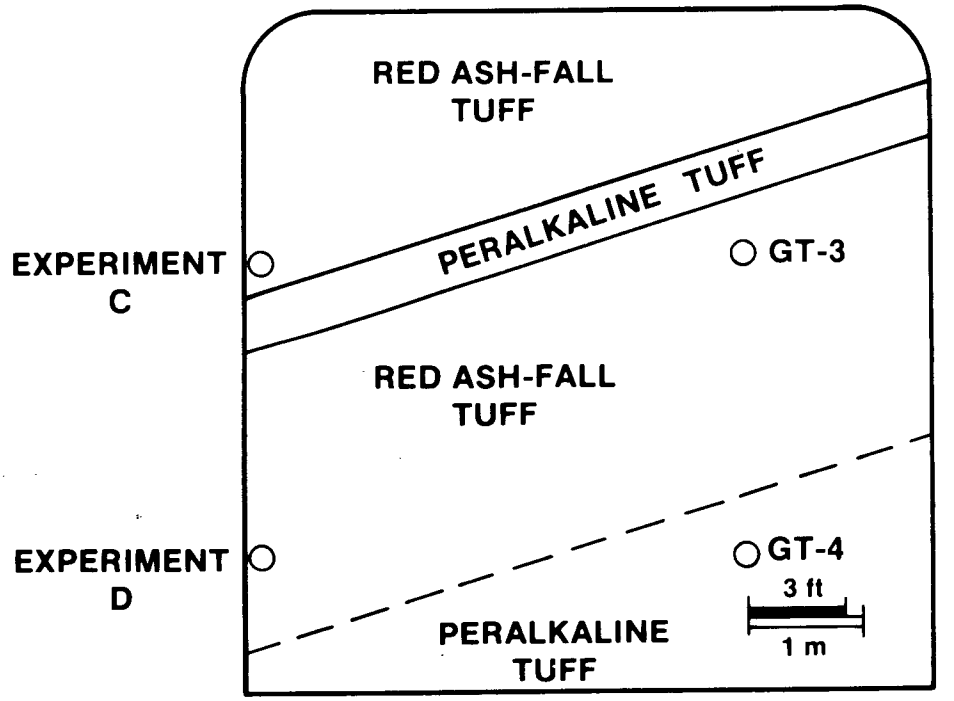

TEST SERIES #2

Figure 5. Schematic of Mined-Back Drift Face Showing Lithology and Hole Locations for Tests Series #1 and #2

Table 1

Physical Properties of Tuff in the Test Bed
(from Cuderman et al, 1986)

Property	Red Ash-Fall Tuff	Peralkaline Tuff
Density (kg/m^3)	2000	1850
Young's Modulus (GPa)	8.2	3.2
Shear Modulus (GPa)	3.4	1.3
Bulk Modulus (GPa)	6.2	1.6
Poisson's Ratio	0.27	0.19
Compressive Wave Velocity (m/s)	2590	2500
Shear Wave Velocity (m/s)	1670	1500
Compressive Strength (MPa) (Unconfined)	22	10
Compressive Strength (MPa) (6.895 MPa confining pressure)	39	22
Tensile Strength (MPa)	1.58	0.34

For each experiment, a 0.15-m (6-in) diameter borehole angled at 3.5° below horizontal was drilled into the drift face (Figure 6). Drillholes in Test Series #1 were 12.2 m (40 ft) in length, while those in Test Series #2 and #3 were 7.6 m (25 ft) in length. In all eight experiments, a 0.10-m (4-in) I.D. casing with centralizers was inserted into the borehole and grouted in place. The bottom 2.4 m (8 ft) of casing then was perforated using 10-g (0.35-oz) charges. A hollow carrier gun was used for perforating in all except Experiment H; in Experiment H, a strip gun was used.

The number, size, and phasing of perforations varied from experiment to experiment. Values of key parameters in each experiment are tabulated in Table 2. Comparison of the physical characteristics of the various propellants used is provided in Table 3.

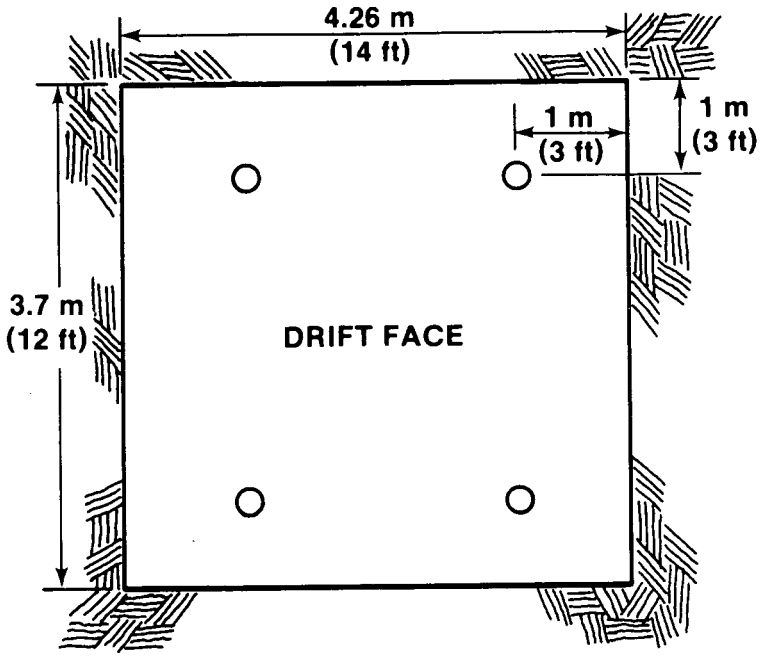

EMPLACEMENT VIEW

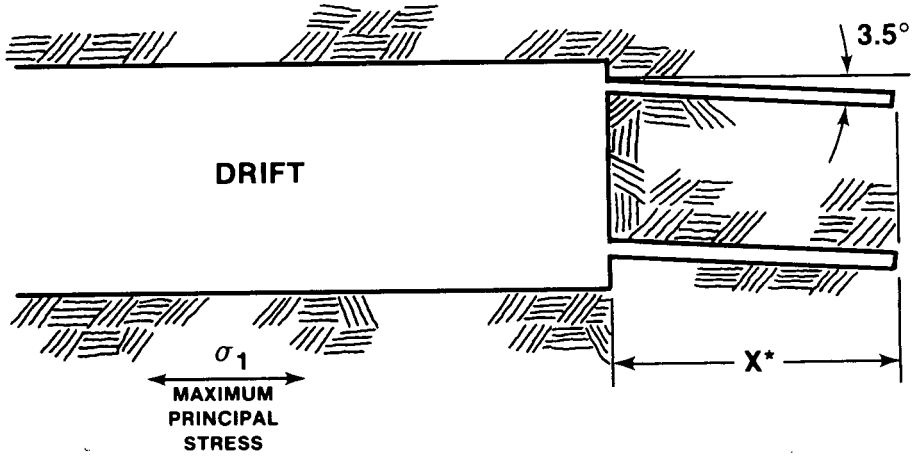

*FOR TEST SERIES #1, X EQUALS 12.2 m (40 ft)
FOR TEST SERIES #2 AND #3, X EQUALS 7.6 m (25 ft)

ELEVATION VIEW

Figure 6. Schematic of Borehole Placement Relative to the Drift Face

Table 2

Values of the Variable Parameters in the Experiments A Through H

Experiment	Borehole Depth (m [ft])	Fluid-Filled/ Fluid-Free	Perforations			Propellant		Canister O.D. (m [in])
			Perfs per meter (ft)	Perf Diameter (mm [in])	Phasing (deg)	Type	Weight (kg [lb])	
A	12.2 (40)	Free	13 (4)	9.5 (0.375)	120	M5B	2.15 (4.75)	0.044 (1.75)
B	12.2 (40)	Free	13 (4)	9.5 (0.375)	120	M5A	1.81 (4.00)	0.044 (1.75)
C	7.6 (25)	Free	13 (4)	9.5 (0.375)	90	M5B	2.72 (6.00)	0.044 (1.75)
D	7.6 (25)	Filled	13 (4)	9.5 (0.375)	90	M5B	2.38 (5.25)	0.044 (1.75)
E	7.6 (25)	Filled	20 (6)	15 (0.6)	120	M30B	4.65 (10.25)	0.068 (2.66)
F	7.6 (25)	Filled	20 (6)	15 (0.6)	120	M5B	5.90 (13.00)	0.068 (2.66)
G	7.6 (25)	Free	20 (6)	15 (0.6)	120	M30B	4.69 (10.35)	0.068 (2.66)
H	7.6 (25)	Filled	13 (4)	9.5 (0.375)	180	M5A	2.09 (4.60)	0.044 (1.75)

Table 3

Comparison of M5 and M30 Propellants
(from Cuderman et al, 1986)

Variable	M5A	M5B	M30B
Grain length (mm)	6.73	11.0	23.75
Grain diameter (mm)	1.40	5.00	11.87
Perforation diameter (mm)	0.33	0.50	1.07
Number of perforations	1	7	7
Density (kg/m^3)	1660	1660	1660
Isochronic flame temperature (K)	3245	3245	3040
Gas production constant (m^3/kg)	0.88	0.88	0.96
Burn rate constant (A)*	0.000761	0.000761	0.00576
Burn rate constant (n)*	0.895	0.895	0.652

*Burn rate $R(m/s) = A[0.175\ P(MPa)]^n$

Hardware used in each experiment included a propellant canister, pressure-transducer canister, packer, and cable tube (Figure 7). The pressure transducers were four-arm, bridge-type, commercially available gages rated at 207 MPa (30,000 psi). The packer, fabricated of lightweight elastomer, confined water to the test zone; an internal pressure of 0.10 to 0.17 MPa (15 to 25 psi) was adequate to confine water to the test zone. The cable tube provided a conduit for instrumentation cables and lines for pressurizing the packer to be routed to the borehole collar.

Two different propellant canister designs were used in the three test series. In Test Series #1, which includes experiments A and B, a polyvinylchloride (PVC) canister filled with propellant was initiated using three exploding bridge-wire (EBW) detonators, each surrounded by about 6 g (0.21 oz) of black powder. While this design had proven adequate for fluid-free boreholes, the design proved unsatisfactory for use in fluid-filled boreholes because of quenching. Subsequent test series used a design (Figure 8) consisting of a section of PVC

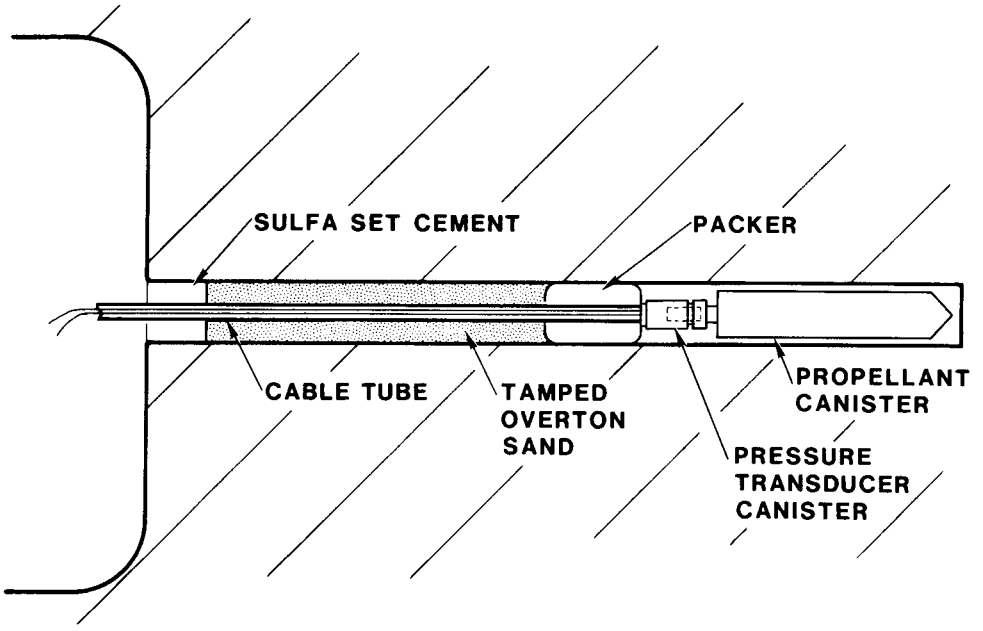

Figure 7. Schematic of Borehole Instrumentation

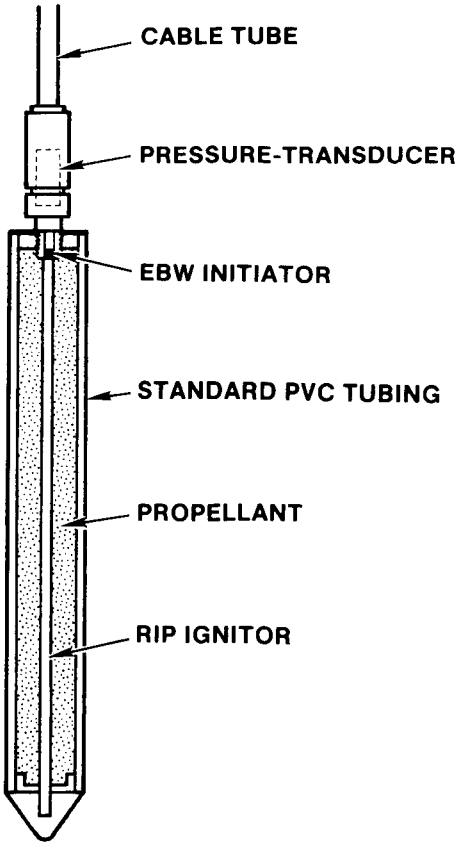

Figure 8. Schematic of Propellant Canister

pipe and a centered rapid ignition primer (RIP) ignitor, with the annulus between ignitor and pipe filled with propellant. One end of the assembly was closed off with an endcap, the other by the pressure transducer assembly. The RIP ignitor is initiated by an exploding bridge-wire initiator; it ignites the entire length of the propellant essentially simultaneously, given that the burn rate of the RIP ignitor is 7000 m/s (23000 ft/s). The RIP had a center core of lead-sheathed mild detonating fuse (MDF) surrounded by B/KNO3 pyrotechnic. The ends of the MDF were terminated with an aluminum endcap containing a small pressing of RDX explosive. A short length of MDF ribbon was sandwiched between two EBW initiators and the RIP endcap. This design provided excellent firing redundancy.

Upon installation of the hardware, water was added to those test zones that were to be liquid-filled, the packer was inflated, and the zone around the cable tube was blown dry. All experiments were stemmed with damp Overton, Nevada, sand. Roughly 0.3 m (1 ft) of a 50/50 weight-percent mixture of sand and sulfate-based cement was placed at the collar to ensure that the stemming remained in the borehole during the test.

3. TEST RESULTS

The HEGF program in cased and perforated boreholes progressed in the sequence: Series #1, Experiment A, Experiment B (followed by GT-1 and GT-2, which used uncased boreholes), mineback of the test bed to reveal fracture patterns; Series #2, Experiment C, Experiment D (followed by GT-3 and GT-4, which used uncased boreholes), mineback of the test bed; and Series #3, Experiments E through H, and mineback of the test bed. Parameters varied among the experiments included number of perforations per meter of casing (perforation density), perforation diameter, perforation phasing relative to the far-field in situ stresses, type and amount of propellant used, and presence or absence of liquid in the borehole (Table 2). Parameters held constant in the experiments included borehole orientation relative to the far-field in situ stresses, borehole diameter, and length of the test zone, which was the bottom 2.4 m (8 ft) of the borehole. Resultant fracture patterns and casing damage are summarized in Figure 9.

Test Series #1 (Experiments A and B)

The two experiments in Test Series #1 involving cased and perforated wellbores (Experiments A and B) were scoping experiments designed to examine the behavior of the HEGF technique when the wellbore is cased and perforated. The experiments were configured with relatively small perforation diameters and number of perforations per meter of casing (Table 2). As a result, only small amounts of propellant gas exited through the perforations during propellant burn. This limited the amount of propellant that could be used because of the desire to avoid badly splitting the casing. Complicating factors such as fluid in the borehole were avoided, and variables other than propellant type were held constant. In both experiments, a 0.044-m (1.75-in) O.D. propellant canister was used and perforations were

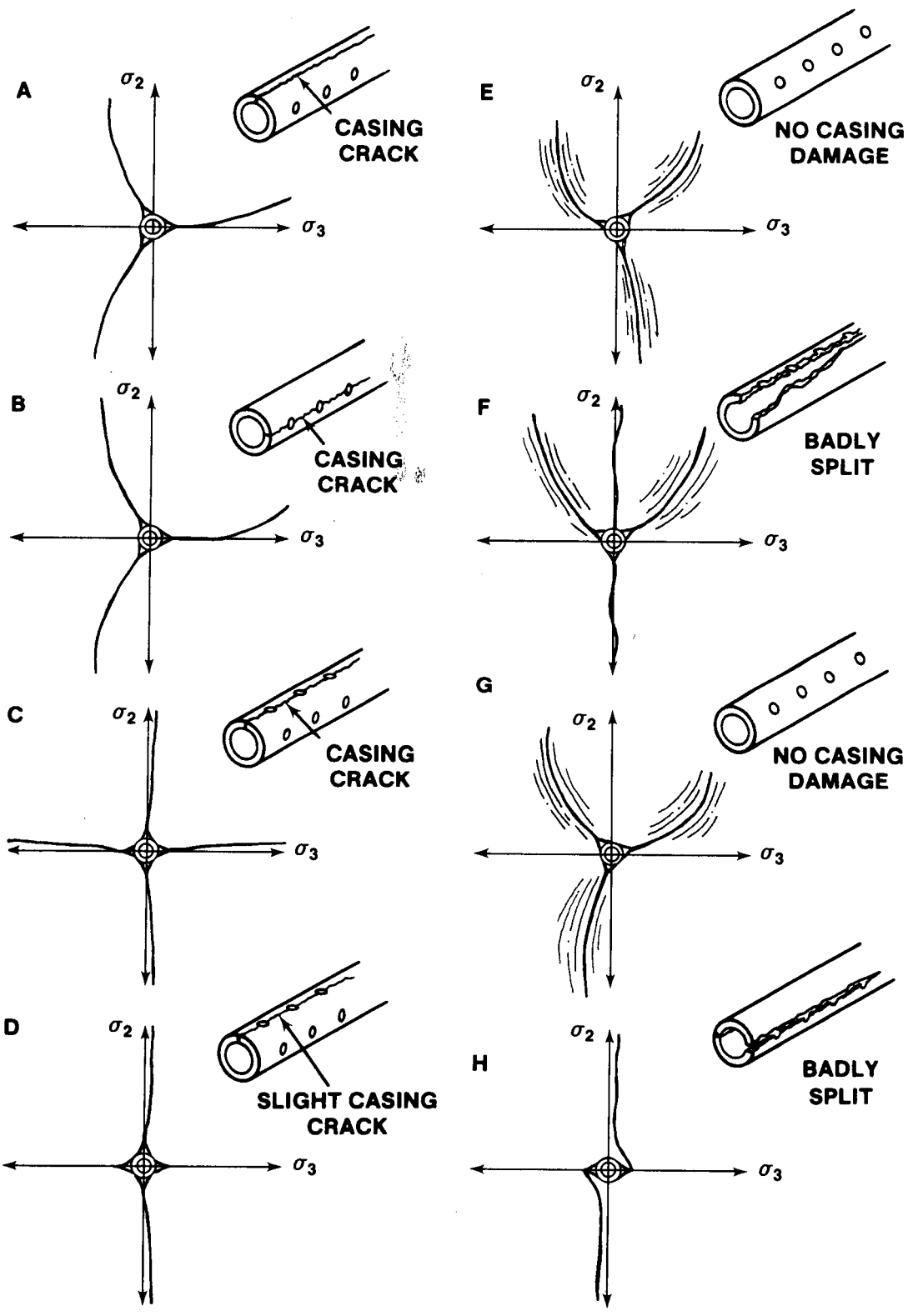

Figure 9. Schematic of Mineback Results from Experiments A Through H Showing Fracture Patterns and Casing Damage

9.5 mm (0.375 in) in diameter, spaced 13 per meter (4 per foot), and placed 120° apart, with one row oriented roughly parallel to σ_3 (Table 2).

In Experiment A, 2.15 kg (4.75 lb) of the slower-burning M5B propellant was initiated using the exploding bridge-wire detonators. No pressure trace was obtained because the cable and cable tube were completely severed at the detector during the shot, presumably very soon after initiation.

Mineback of the test bed showed that a fracture propagated from each line of perforations, as predicted (Figure 9 and 10). Also, as predicted, the fracture orientation curved toward the normal to the minimum in situ stress as the fracture propagated into the surrounding rock. Fracture lengths of up to 1.2 m (4 ft) were observed. A single split occurred, roughly at the top of the casing. However, the split closed after pressurization and no permanent casing deformation occurred.

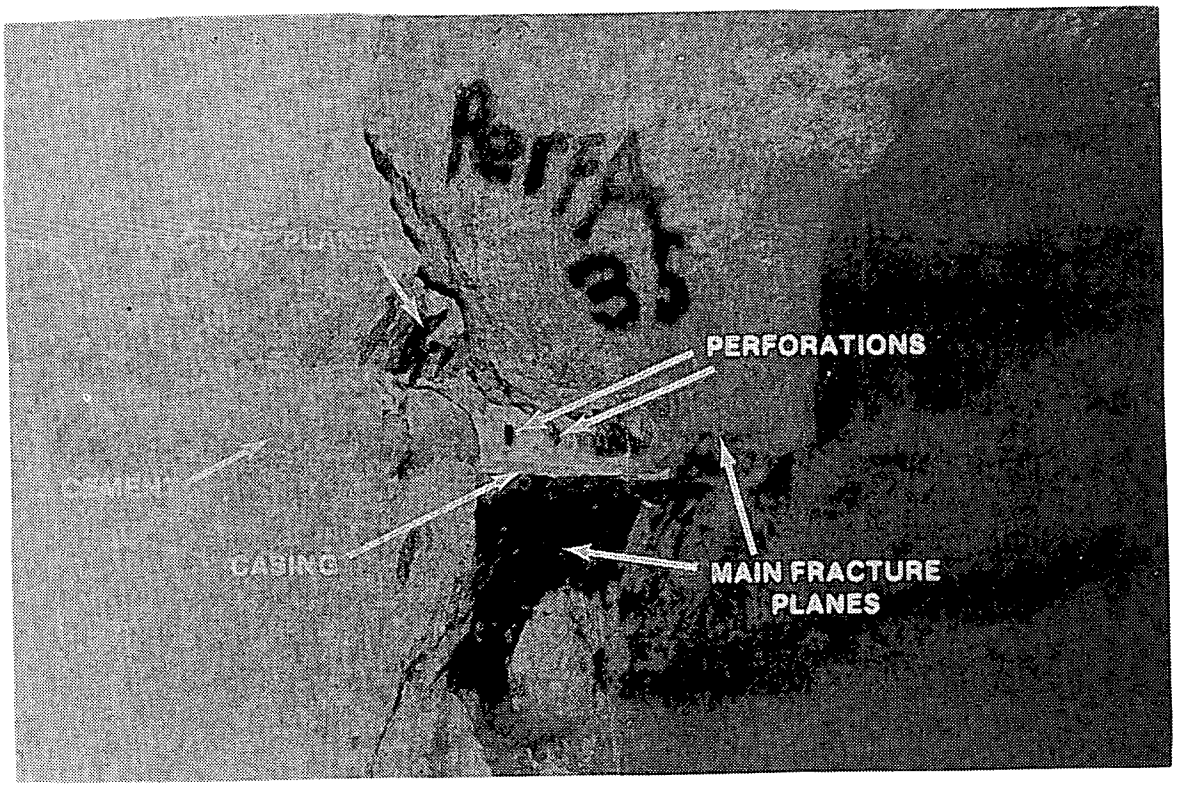

Figure 10. Photograph of Mineback for Experiment A

Experiment B was identical to Experiment A except that 1.81 kg (4.0 lb) of the faster-burning M5A propellant was used. If the premise that minimal gas flow occurred during the propellant burn was correct, then the results of Experiments A and B should yield essentially the same results, given that comparable amounts of propellant were used in both.

The pressure history recorded for Experiment B (Figure 11) showed a pressure risetime of 2 ms and a peak pressure of 130 MPa (20,000 psi). The pressure then dropped, presumably because of pressure loss through perforations and possibly casing fractures, then increased again to band edge at 276 MPa (40,000 psi). Pressures above about 110 MPa (16000 psi) should not have occurred for a 0.044-m (1.75-in) O.D. propellant canister in a 0.10-m (4-in) diameter borehole. Upon reentry, water was observed venting through the cable tube, although the amount could not be determined.

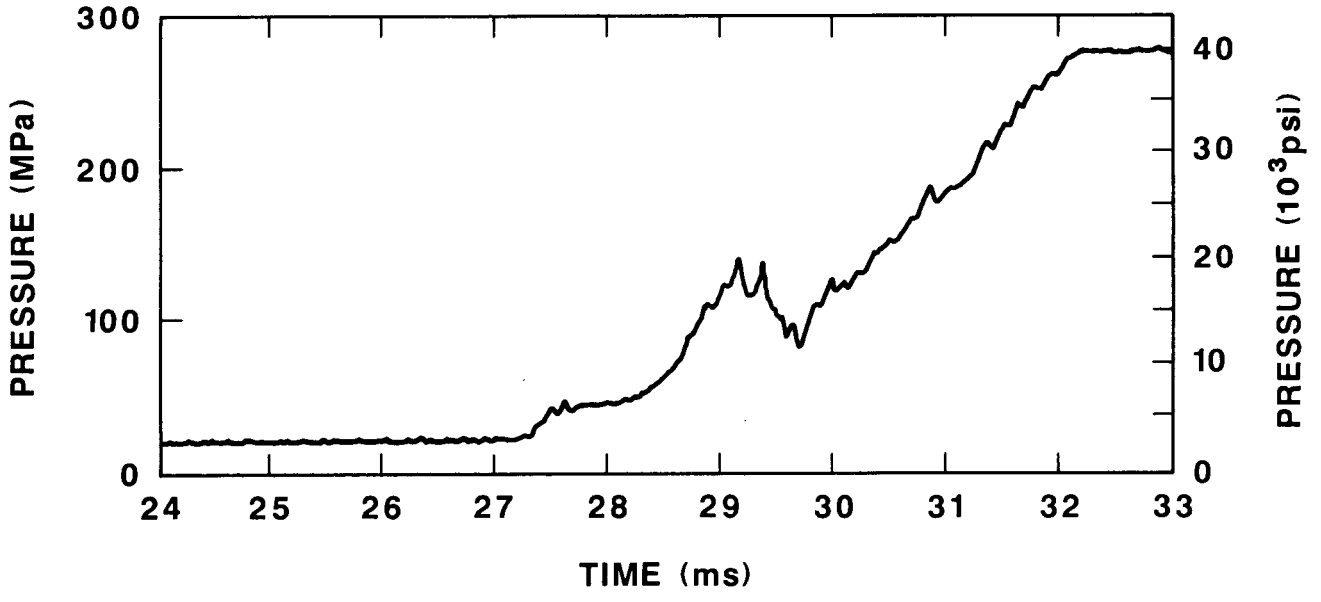

Figure 11. Plot of Pressure History for Experiment B

The fracture geometry was essentially identical to that of Experiment A (Figure 9), thus suggesting that peak pressures in the two experiments were similar. The fracture emanating from the line of

perforations along σ_3 extended 2.13 m (7 ft) into the formation. The other two fractures extended into the side and floor of the drift, respectively, and were not fully exposed to determine their extent (Figure 12). Casing damage was similar to Experiment A except that the crack occurred along the line of horizontal perforations (Figure 9).

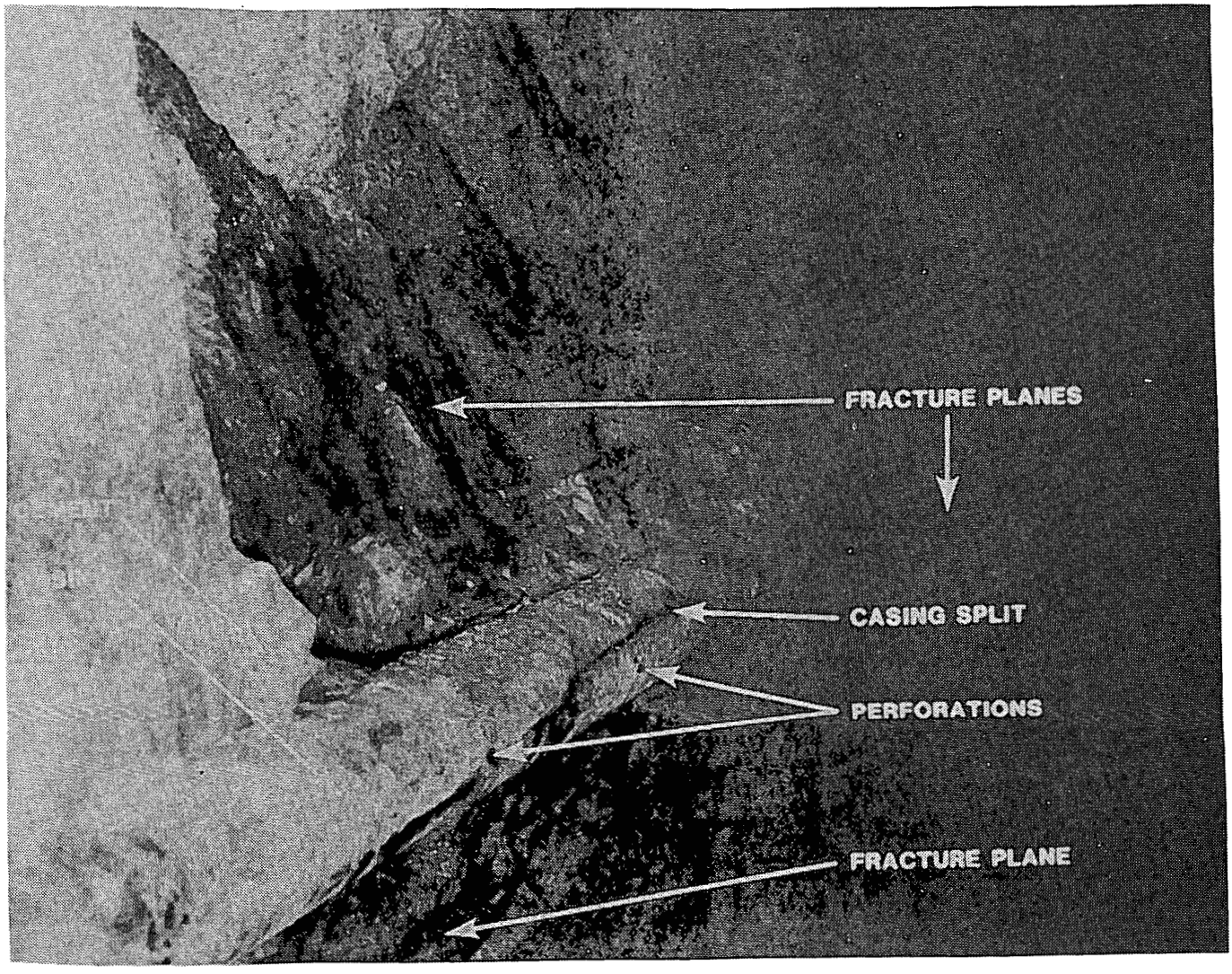

Figure 12. Photograph of Mineback for Experiment B

The pressure history obtained in Experiment B is not consistent with predictions for either a liquid-free or a liquid-filled borehole. Typically in liquid-filled boreholes, the peak pressure is lower and

the risetime faster (Cuderman et al, 1986) than observed in Experiment B. The presence of water in Experiment B should have yielded a lower peak pressure, not a higher one than predicted. Examination of the data and the instrumentation setup revealed nothing that would account for the anomalous pressure record, given the fracturing obtained.

Test Series #2 (Experiments C and D)

The two experiments in Test Series #2 involving cased and perforated wellbores (Experiment C and D) were designed to investigate the effect of perforation phasing and orientation on fracturing obtained, as well as the effect on fracturing when the borehole is filled with liquid. In both experiments, the lines of perforations were oriented parallel to the maximum and minimum in situ stresses, resulting in a 90° phasing (Figure 9). Parameters such as number of perforations per unit length, perforation diameter, and propellant-canister diameter matched those of Experiments A and B (Table 2). Because similar results were obtained in Experiments A and B, using M5B and M5A propellants, respectively, M5B was chosen for both Experiment C and Experiment D.

In Experiment C, the borehole was liquid-free and loaded with 2.72 kg (6.0 lb) of M5B propellant. The resultant pressure record appears in Figure 13. Mineback of the test bed uncovered a fracture from each line of perforations (Figure 14). Casing damage was similar to that in Experiment A, with a crack occurring along the 90° (vertical) perforation line, corresponding to the plane normal to the minimum far-field principal in situ stress plane (Figure 9).

Experiment D was essentially identical in design to Experiment C except that the borehole was filled with water. The initiation of 2.38 kg (5.25 lb) of M5B propellant produced the pressure curve plotted in Figure 15. Mineback of the test bed uncovered fractures only from the two lines of perforations oriented normal to the minimum far-field in situ stress plane (Figures 9 and 16). The absence of fractures normal to the maximum far-field in situ stress plane is consistent with results obtained from uncased, fluid-filled boreholes (Cuderman et al, 1986).

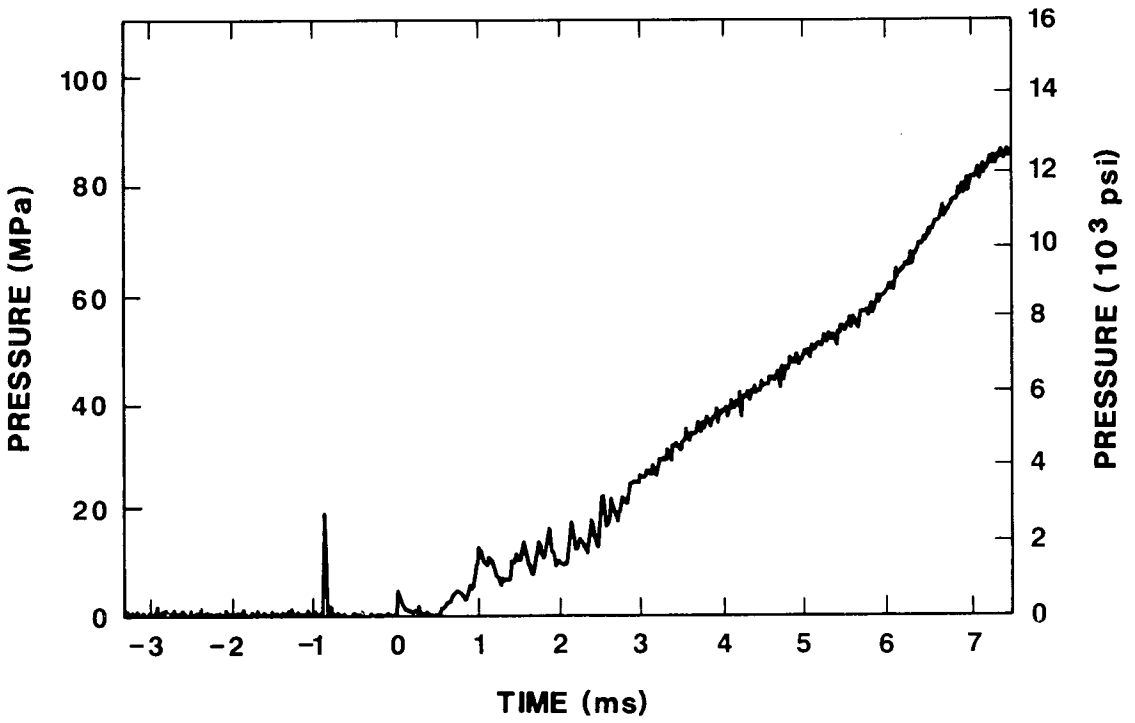

Figure 13. Plot of Pressure History for Experiment C

Figure 14. Photograph of Mineback for Experiment C

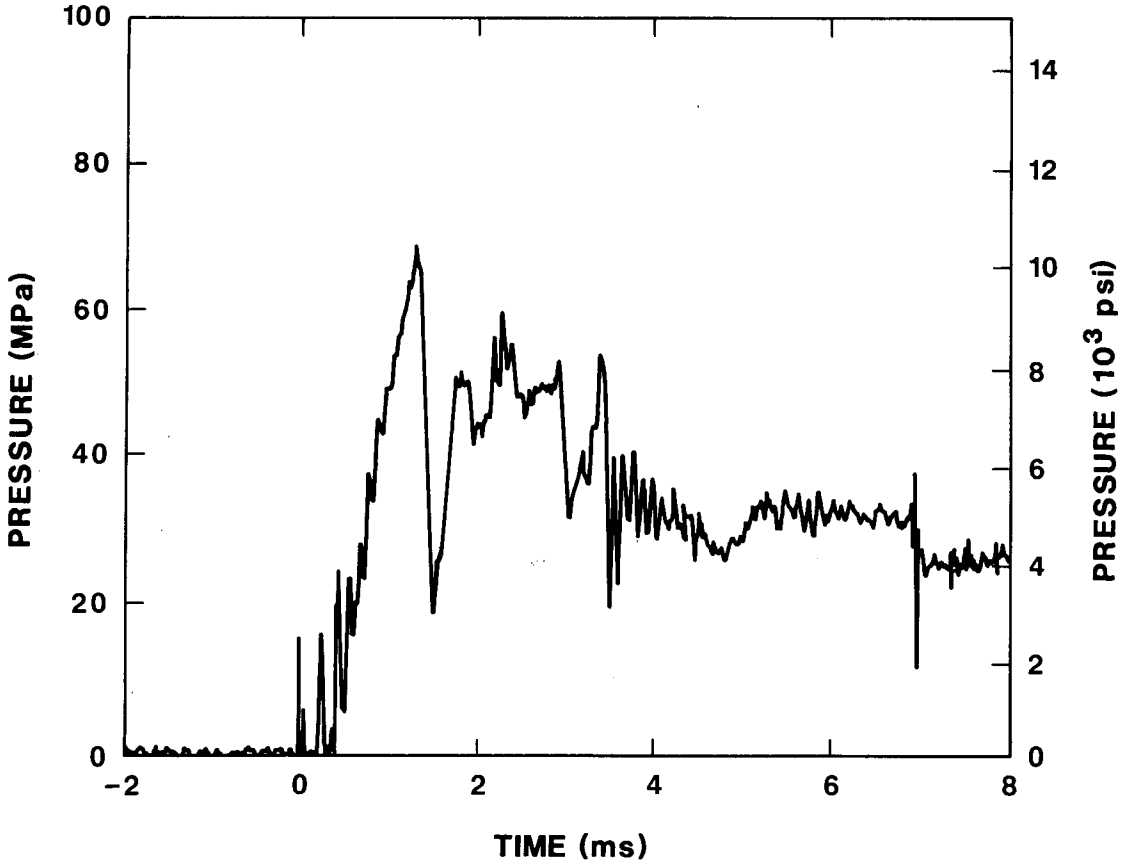

Figure 15. Plot of Pressure History for Experiment D

It was postulated that the orientation of the perforations along principal planes of stress should yield longer fractures than the random orientation obtained with 120° phasing. The mineback results showed that this was marginally the case. However, the fact that the set of fractures perpendicular to the maximum principal stress in the water-filled borehole did not propagate suggests that such an oriented geometry in a liquid-filled wellbore may not be as effective as the more random 120° phasing.

Test Series #3 (Experiments E Through H)

In evaluating factors controlling fracturing through cased and perforated wellbores, Test Series #1 and #2 provided empirical data for cases where perforations were relatively small (9.5 mm

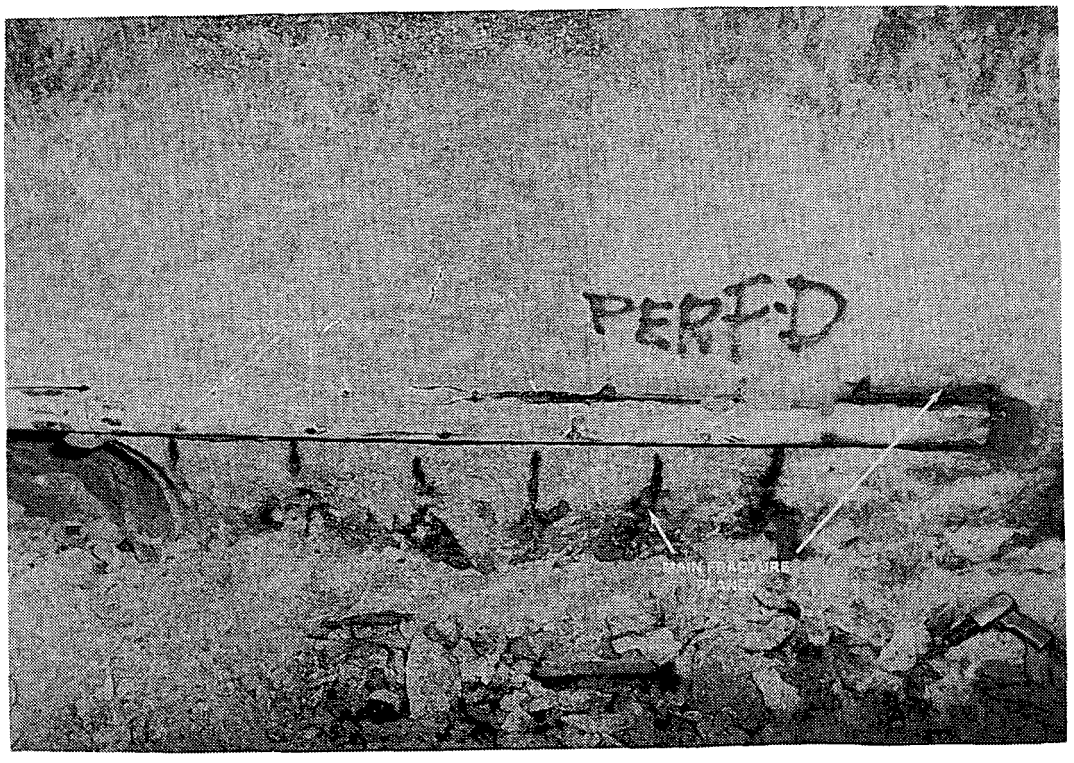

Figure 16. Photograph of Mineback for Experiment D

[0.375 in]), not closely spaced (13 per meter [4 per foot]), and oriented either with 120° phasing or along principal in situ stress planes with 90° phasing. Propellant charges were relatively small and the propellant used was relatively small grained and fast burning (Table 3). The objective of Test Series #3 basically was to provide empirical data for cases where

- perforations were larger in diameter and spaced in such a manner as to produce the maximum practical perforation density
- propellant charges were as large as possible, given that wellbore damage was to be avoided
- large-grained, slow-burning propellants were compared to smaller-grained, faster-burning propellants, given that other variables were held constant.

For Test Series #3, the number of perforations per meter of casing in Experiments E, F, and G was increased from the 13 used in Test Series #1 and #2 to 20 (4 per foot to 6 per foot). Perforation diameter was increased from 9.5 to 15 mm (0.375 to 0.6 in).

Propellant-canister size was increased from 0.044-m (1.75-in) O.D. to 0.068-m (2.66-in) O.D., which essentially doubled the quantity of propellant present. A 120° perforation phasing was used in all three tests (Figure 9) because the results of Test Series #1 and #2 did not indicate a significant fracturing improvement for 90°-phased perforations oriented along principal far-field stress planes. Perforation lines generally were oriented in the manner that optimized observation of fractures during mineback.

The design of Experiment H was the one exception to the basic goal of Test Series #3. In Experiment H, parameters such as perforations per unit length, perforation diameter, propellant weight, and canister diameter closely matched those of Test Series #1 and #2. The objective in Experiment H was to induce fractures only in the plane of the minimum far-field in situ stress (σ_3), i.e., normal to the hydraulic fracture direction. Successful generation of these fractures would demonstrate that the HEGF technique could produce fractures in any direction desired.

Experiments E and G -- Experiments E and G were essentially identical except that the borehole in Experiment E was water-filled and the borehole in Experiment G was liquid-free. The objective of these two experiments was to produce large fracture surfaces from the three lines of perforations with no attendant casing damage. The propellant used was the relatively large-grain, slow-burning M30B propellant.

The pressure trace for Experiment E (Figure 17a) shows the 4.65 kg (10.25 lb) of M30B propellant produced a pressure risetime of approximately 6 ms and a peak pressure of 86.9 MPa (12,600 psi). The pressure trace for Experiment G (Figure 17b) shows the 4.69 kg (10.35 lb) of M30B propellant produced a pressure risetime of 13.9 ms and a peak pressure of 114 MPa (16,500 psi). As in the case of Experiments C and D, the results are consistent with those from uncased, liquid-filled boreholes, where pressure risetimes were found to be considerably faster and peak pressures considerably lower than those measured in liquid-free, uncased boreholes (Cuderman, 1986a).

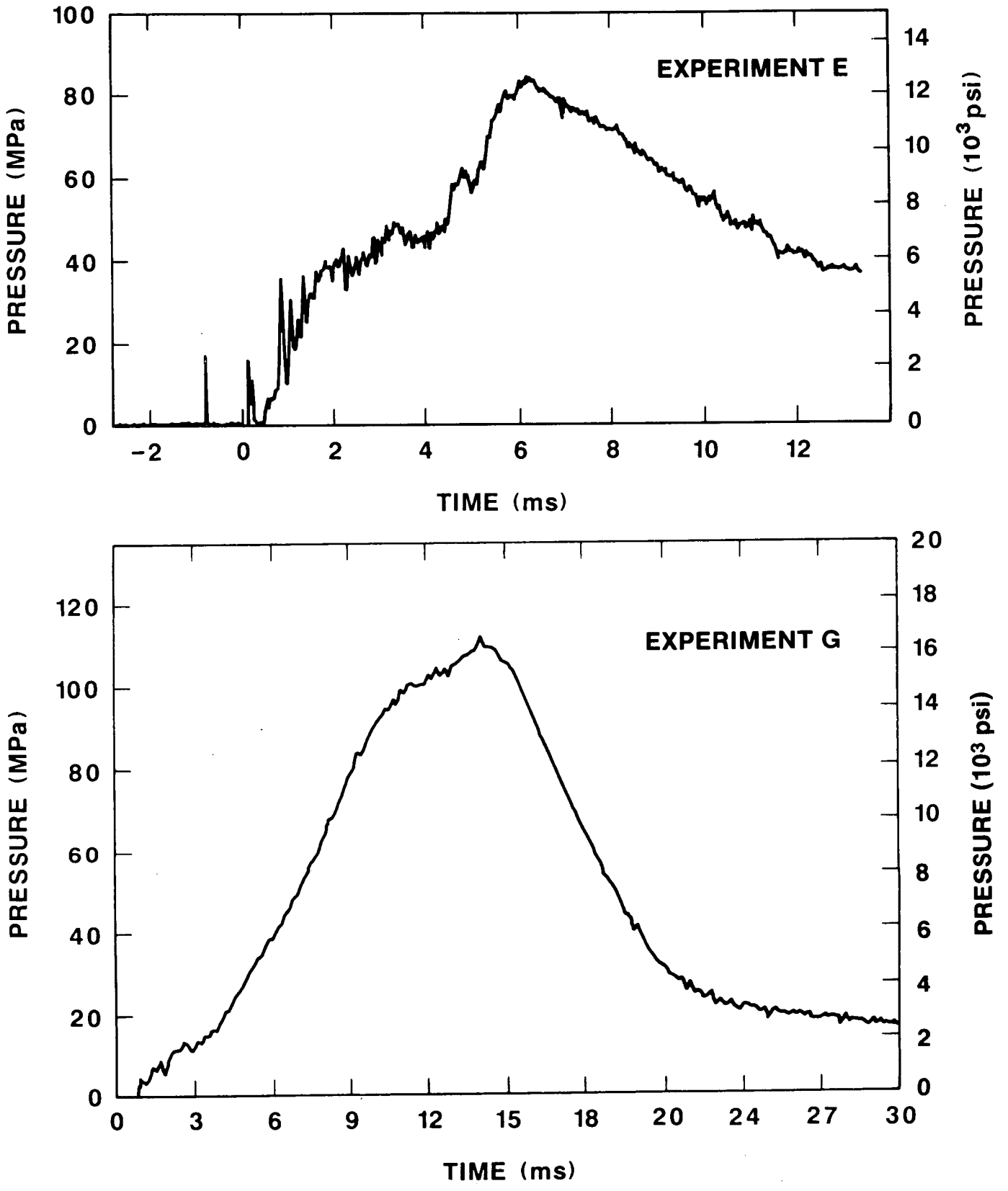

Figure 17. Plot of Pressure History for Experiments E and G

Fracture patterns observed in mineback for both Experiment E and Experiment G were generally similar to those observed in Experiments A and B (Figures 9, 18, and 19). Fractures emanated from each line of perforations and bent toward the plane normal to minimum in situ stress as distance from the borehole increased.

Figure 9 portrays diagrammatically the fracturing obtained in the two experiments. A new phenomenon observed in the fracture patterns for Experiments E and G was the presence of a number of smaller fractures that parallel the three main fractures. Similar satellite fractures were not observed in Test Series #1 and #2. As noted previously, Test Series #3 was conducted in the PTE 2 drift, while Test Series #1 and #2 were conducted in the MAC drift. One difference noted during mineback of Test Series #3 was a significantly greater tendency toward rock slabbing than in the MAC drift. The parallel fractures thus may be due to differences in rock fabric in the PTE 2 drift.

Experiments E and G were successful in that no splitting of the casing or casing deformation occurred, regardless of whether or not fluid was present in the borehole. The conclusion drawn from these experiments was that the combination of relatively slow propellant, maximum practical perforation diameter, and maximum practical perforation density result in well-defined fractures from each line of perforations with no attendant casing damage. This is true even when a relatively large quantity of propellant is used.

Experiment F -- The objective of Experiment F was to determine the effect of propellants with faster pressurization rates on casing damage when perforations are relatively large and there is a high density of perforations per unit length of casing. As a result, Experiment F was essentially identical to Experiment E except that the faster-burning M5B propellant was used in Experiment F. Because of the smaller grain size and higher packing density of M5B propellant relative to M30B propellant, more propellant (5.90 kg [13.00 lb] versus 4.65 kg [10.25 lb] in Experiment E) fit into the 0.068-m (2.66-in) O.D. in Experiment F.

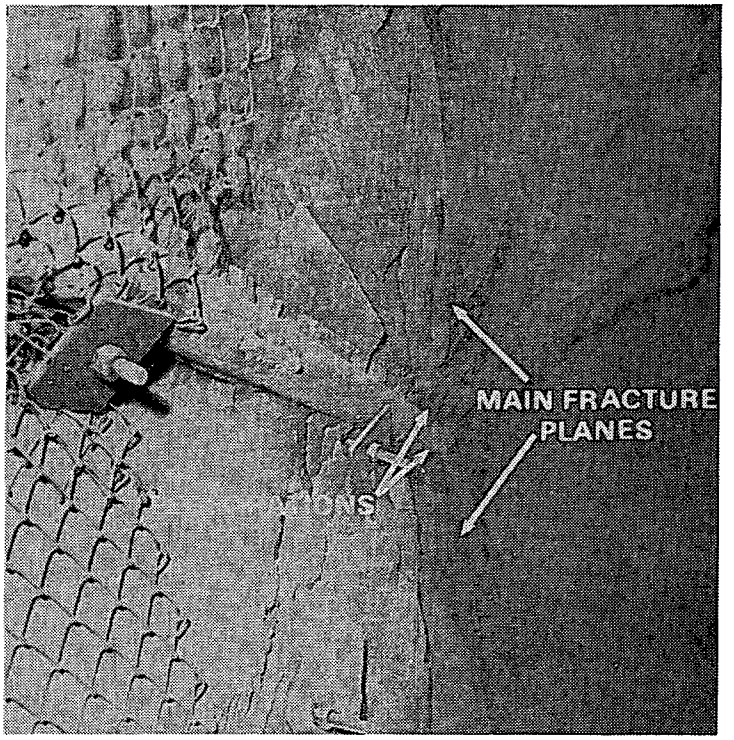

Figure 18. Photograph of Mineback of Experiment E

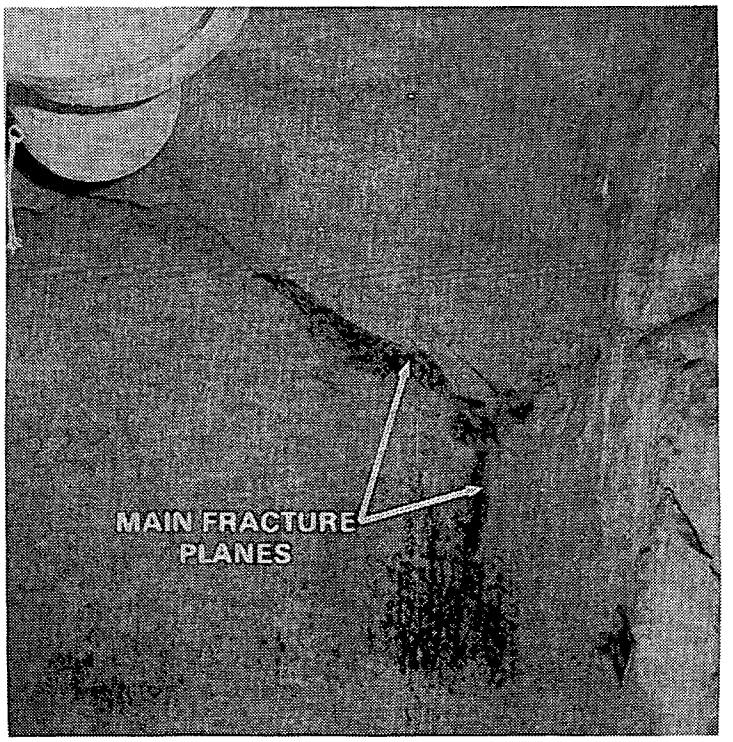

Figure 19. Photograph of Mineback of Experiment G

The pressure history for Experiment F is presented in Figure 20. The pressure trace shows a pressure risetime of 0.12 ms and a peak pressure of 114 MPa (16,500 psi). Note the oscillations in the pressure trace, which are similar to oscillations observed in uncased, fluid-filled boreholes (Cuderman, 1986a).

Mineback of the test bed revealed a fracture along each line of perforations but extensive, clearly unacceptable casing damage along the line of perforations closest to the plane normal to σ_3 (the hydraulic-fracture direction) (Figures 9 and 21). A fourth fracture emanated from the split in the casing and also propagated along the plane normal to the minimum far-field in situ stress (Figure 9).

The extensive casing damage and hydraulic fracture emanating from the split indicates that given the perforation parameters selected, the amount of propellant used, and fluid in the borehole, M5B propellant pressurizes the borehole too rapidly to avoid casing damage.

Experiment H -- As noted previously, the objective of Experiment H was to determine whether fractures would propagate from perforations if all were oriented along σ_3, i.e., normal to the hydraulic-fracture direction. Recall that in fluid-filled Experiment D, fractures failed to form in the plane normal to the hydraulic-fracture plane, but fractures did form in the plane normal to the hydraulic-fracture plane in liquid-free Experiment C. Experiment H was designed to closely match Experiment D, except that perforation phasing was 180°, with all perforations oriented along σ_3, and faster-burning M5A propellant was used. M5A propellant was chosen to delimit conditions under which the relatively fast-burning propellant produces acceptable results.

Initiation of the 2.09 kg (4.60 lb) of M5A propellant produced the pressure trace plotted in Figure 22. Mineback of the test bed revealed that fractures formed along the lines of perforations, but instead of propagating along σ_3, the fractures propagated around the casing and then in the hydraulic-fracture direction, even though there were no perforations in that direction (Figures 9 and 23). An additional fracture propagated from the end of the borehole, a result

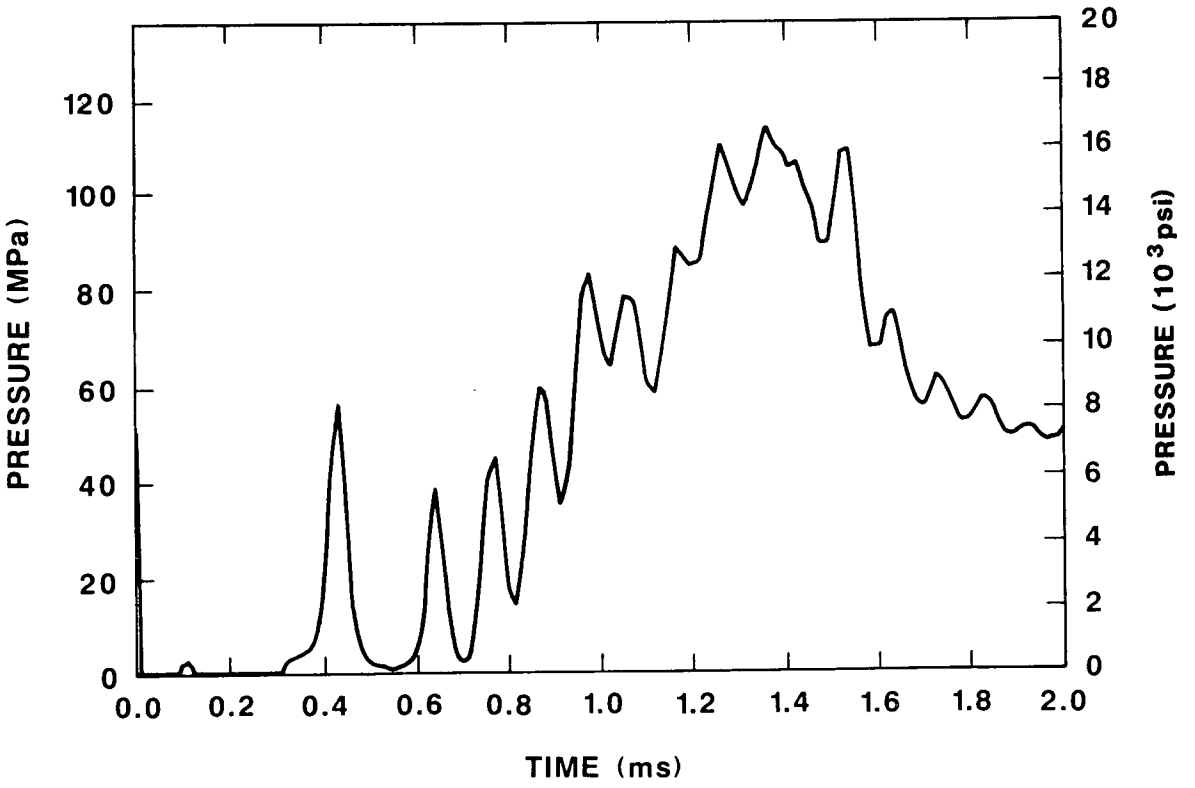

Figure 20. Plot of Pressure History for Experiment F

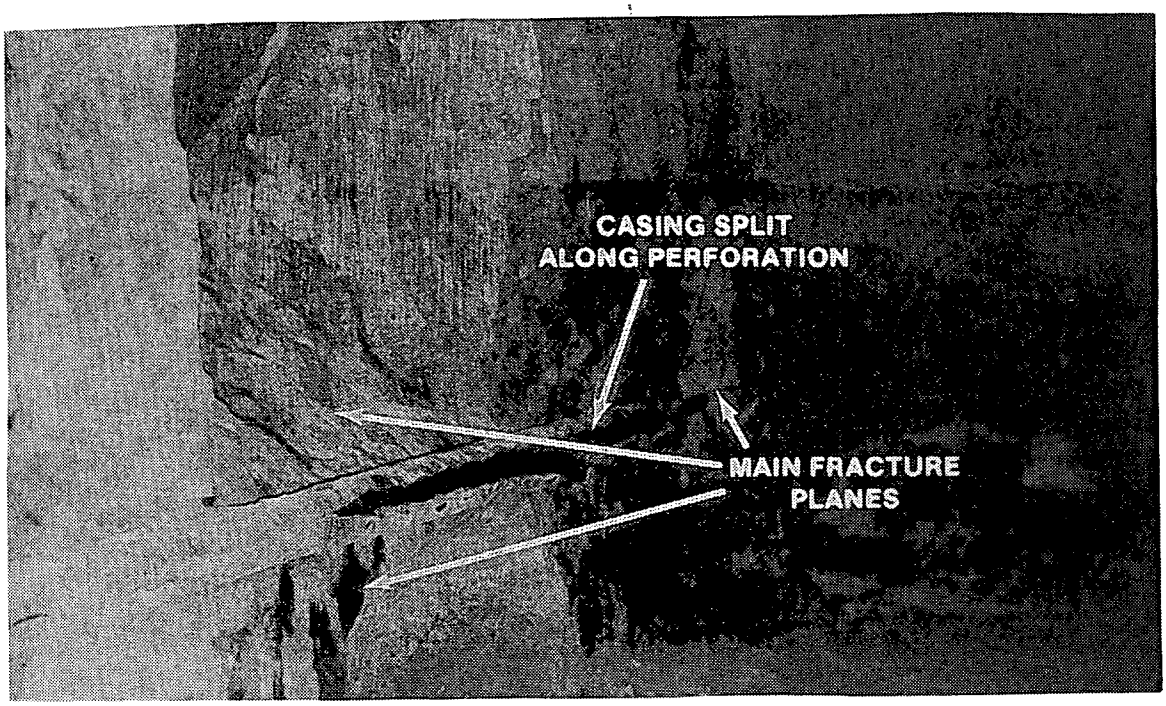

Figure 21. Photograph of Mineback for Experiment F

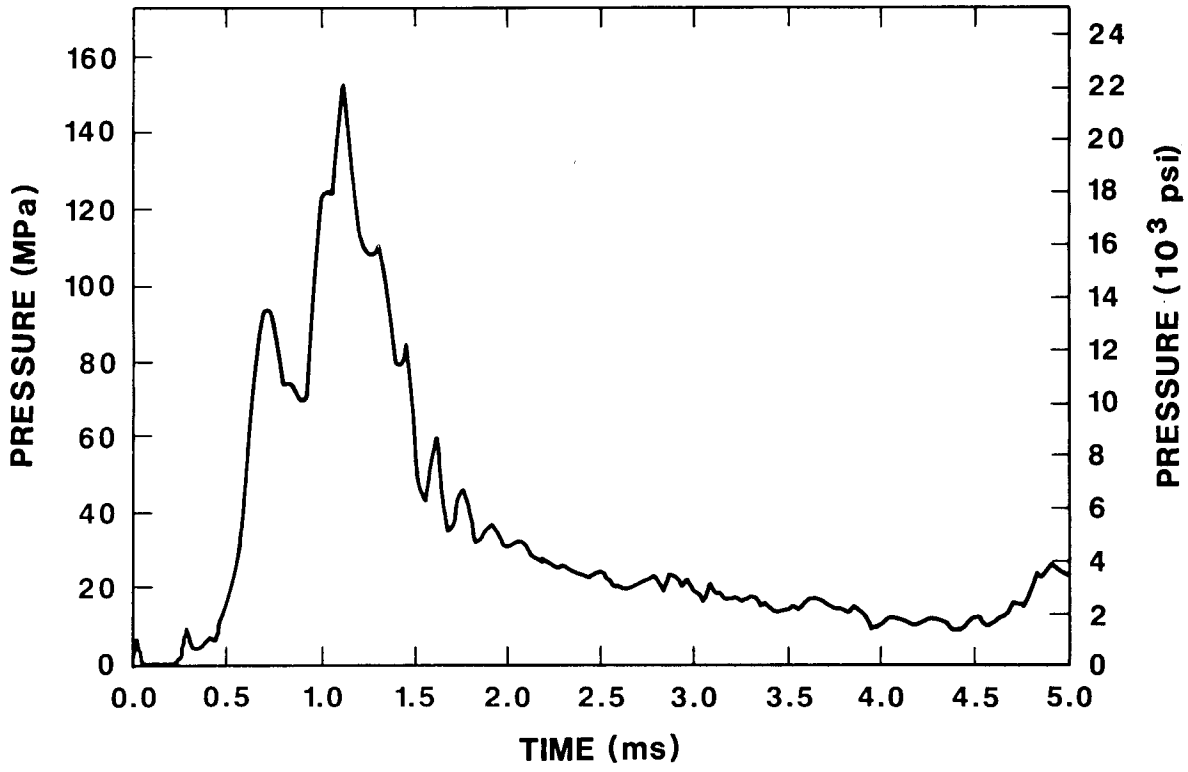

Figure 22. Plot of Pressure History for Experiment H

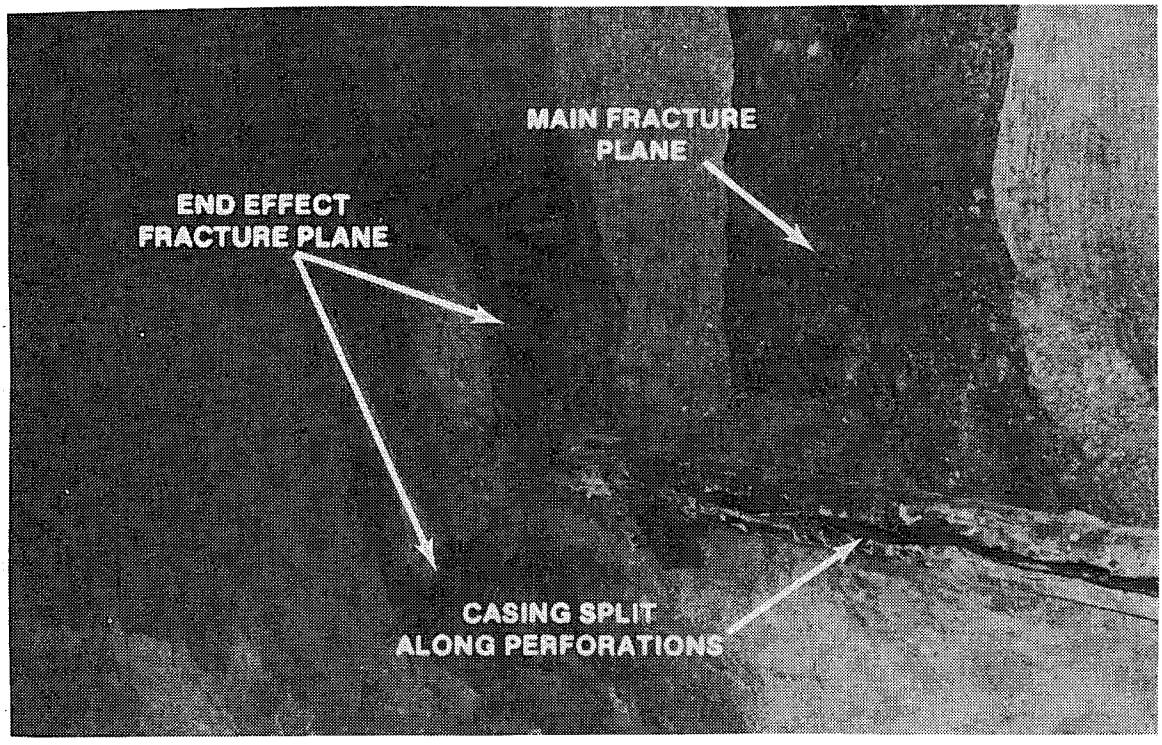

Figure 23. Photograph of Mineback for Experiment H

similar to that observed in uncased fluid-filled boreholes (Cuderman et al, 1986). Casing damage was severe, with a split and separation observed along the perforation lines.

Several factors may have contributed to the surprising result. A 180° strip gun was used to produce the 9.5-m (0.375-in) perforations in the casing of Experiment H. These perforations were not as large as those obtained with the hollow carrier gun used in Experiments A through G. Smaller perforations mean less propellant gas vents from the borehole, resulting in an increased risk of severe fracturing of the casing.

Secondly, the presence of fluid in the borehole, particularly when faster-burning propellants are used, seems to encourage the formation and propagation of fractures normal to σ_3 (the hydraulic-fracture direction). Results from Experiment H are similar to those of Experiment D, which also was water filled and used M5 propellant, in the sense that fractures emanated from the hydraulic-fracture direction but not from perforations parallel to σ_3. Additional experiments with larger, more closely spaced perforations oriented parallel to σ_3, with slower-burning propellants such as M30, and both with and without fluid in the borehole are needed to ascertain whether it is possible to create a single fracture plane normal to the hydraulic fracture direction and to determine the conditions under which this might be achieved.

4. SUMMARY AND CONCLUSIONS

Experiments A through H demonstrated that multiple fractures can be obtained through perforated wellbores with minimal casing damage. Experiments E and G showed essentially identical fracturing for both liquid-free and liquid-filled wellbores of the same geometry. Experiments E and G demonstrated that use of the largest practical perforation diameter and spacing is desirable.

Slower propellants are advantageous because more propellant can escape during the propellant burn time. Use of the slower propellant also permits the use of larger propellant charges. Even with the 0.068-m (2.66-in) O.D. propellant canister, multiple fractures were produced through perforations in Experiments E and G with no casing damage.

The M30B propellant burn rate may be nearly optimal for use in large-perforation, high-perforation-density applications. If the burn rate were much slower, it is likely that only a single hydraulic- type fracture would be initiated from perforations nearest the hydraulic fracture direction. For faster burn rates, such as in Experiment F, severe casing damage results. A slightly larger propellant charge than that used in Experiments E and G might be possible for larger casing sizes.

The preference for fracturing only in the hydraulic fracture direction in water-filled experiments with perforations oriented along principal planes of stress (Experiments D and H) was unexpected. This may indicate that the more random 120° phasing results in more predictable fracture behavior. Additional experiments with slower propellants and more open perforation geometries are required to

determine whether the 90°- and 180°-phased and oriented geometries can be used for effective fracture control in liquid-filled wellbores. However, in the water-filled Experiment F, fractures along lines of perforations phased at 120° propagated as expected, even with severe casing damage.

The fracturing model proposed correctly describes the behavior of propellant-induced multiple fracturing through cased and perforated wellbores when the maximum far-field principal in situ stress is oriented parallel to the borehole. Additional experiments are required to test the model's validity for cases where other borehole orientations are selected. One particularly interesting experiment would involve a borehole oriented parallel to the minimum far-field principal in situ stress. The model predicts fractures normal to the axis of the borehole.

5. ACKNOWLEDGEMENTS

Useful discussions with Dave Northrop, Jim Dunn, and Dave Glowka are gratefully acknowledged. The efforts of an additional number of individuals in organizations at Sandia National Laboratories and from REECo and EG&G contributed significantly to the experiment fielding effort. These include John Patrick, John Talbutt, and Dave Amsler, project engineering and coordiation; Don Werner, Larry Skenandore, and Harold Roberts, AF&F; Ken Melloy and Carl Crowe, data acquisition; Mike O'Brien, geological support; Cris Salinas, photography; and Carl Davis, borehole tv coordination.

6. REFERENCES

Cuderman, J. F., 1984a, "High Energy Gas Fracturing Development," Final Report to Gas Research Institute, GRI-84-0090, SAND84-0247, Sandia National Laboratories Report, Albuquerque, New Mexico, 190 p.

Cuderman, J. F., and Northrop, D. A., 1984, "A Propellant-Based Technology for Multiple Fracturing Wellbores to Enhance Gas Recovery: Application and Results in Devonian Shale," SPE/DOE/GRI 12838, in Proceedings of 1984 SPE/DOE/GRI Unconventional Gas Recovery Symposium, Pittsburgh, PA, May 13-15, pp. 77-86.

Cuderman, J. F., 1984b, "Rock Mechanics Effects Observed Subsequent to Multiple Fracturing of Wellbores," in Proceedings of 25th Symposium on Rock Mechanics, Evanston, IL, June 25-27, 1984.

Cuderman, J. F., 1984c, "Application of a New Multiple Fracturing Technique to Enhance Gas Production in Devonian Shale," in Proceedings of 1984 International Gas Research Conference, Washington, DC, September 10-13, 1984.

Cuderman, J. F., Chu, T. Y., Jung, J., Jacobson, R. D., 1986, "High Energy Gas Fracture Experiments in Fluid Filled Boreholes--Potential Geothermal Application," SAND85-2809, Sandia National Laboratories Report, Albuquerque, New Mexico.

Cuderman, J. F., 1986a, "Effects of Wellbore Liquids in Propellant-Based Fracturing," in Proceedings of 27th U.S. Symposium on Rock Mechanics, University, AL, June 23-25, 1986.

Cuderman, J. F., 1986b, "Tailored-Pulse Fracturing in Cased and Perforated Boreholes," in Proceedings of SPE/DOE 1986 Unconventional Gas Technology Symposium, Louisville, KY, May 18-21, 1986.

Jaeger, J. C. and Cook, N. G. W., 1979, Fundamentals of Rock Mechanics, Chapman and Hall, London.

Distribution:

J. R. White
U.S. Department of Energy
FE 33 GTN D-106
Washington, DC 20545

D. Uthus
U.S. Department of Energy
Office of Oil, Gas and Shale Technologies
Mail Stop D-107
Washington, DC 20545

U.S. Department of Energy (3)
Geothermal Technology Division
Forrestal Building, CE 324
Washington, DC 20545
Attn: M. J. Reed
R. S. Toms
M. Skala

U.S. Department of Energy (5)
Morgantown Energy Technology Center
Box 880 Collins Ferry Road
Morgantown, WV 26505
Attn: A. A. Pitrolo
W. Little
C. A. Komar
K. H. Frohne
J. Duda

G. P. Tennyson
Energy Technologies Division
Albuquerque Operations Office
U.S. Department of Energy
P.O. Box 5400
Albuquerque, NM 87115

U.S. Geological Survey (2)
Box 25046
Denver Federal Center
Denver, CO 80225
Attn: B. E. Law, MS 971
C. W. Spencer, MS 940

J. A. Albright
Earth & Space Science Division
Ess-4
Los Alamos National Laboratory
Los Alamos, NM 87545

Lawrence Livermore National Laboratory (2)
MS L-200
Livermore, CA 94550
Attn: F. Heuze
R. Swift

CER Corporation (2)
Box 15090
Las Vegas, NV 89114
Attn: R. L. Mann
P. Branagan

L. F. Elkins
3412 N. Preston
Oklahoma City, OK 73122

R. W. Veatch
Amoco Production Co.
Research Department
P.O. Box 591
Tulsa, OK 74102

D. E. Nierode
Exxon Production Research
P.O. Box 2189
Houston, TX 77001

Mobil Research & Development Corporation (3)
P.O. Box 819047
Dallas, TX 75381
Attn: J. L. Fitch
M. Strubhar
L. Stowe

S. A. Young
Mobil Oil Corporation
P.O. Box 5444
Denver, CO 80217

R. J. Saucier
Shell Western E&P
Suite No. 7560
Box 576
Houston, TX 77001

R. Veghte
Chandler & Associates
Suite 1400
1860 Lincoln Street
Denver, CO 80203

M. Friedman
Department of Geology
Texas A&M University
College Station, TX 77843

S. Pye
Union Geothermal Division
Union Oil Company of California
P.O. Box 1805
Indio, CA 92201

B. J. Livesay
2616 Angell Avenue
San Diego, CA 92122

J. Combs
Senior Vice President
Geothermal Resources Int'l.
545 Middlefield Road
Suite 200
Menlo Park, CA 94025

R. Rinaldi
Resource Technology, Inc.
4555 South Harvard
Tulsa, OK 74137

1625 Associates, Inc. (2)
1625 Larimer St.
Suite 2107
Denver, CO 80202
Attn: I. H. Cram, Jr.
W. S. Davison

Bell Petroleum Services (2)
P.O. Box 2988
Midland, TX 78702
Attn: E. E. Runyan
K. DeGough

Gas and Oil Management, Inc. (2)
6200 Plateau Drive
Englewood, CO 80111
Attn: K. J. Touryan
R. S. Passamaneck

TPL, Inc. (3)
3409 Bryn Mawr, NE
Albuquerque, NM 87110
Attn: H. M. Stoller
M. Perry
F. Holz

Schlumberger Well Services
P.O. Box A
Rosharon, TX 77583
Attn: L. S. Behrmann
P. M. Halleck

M. O'Brien
Fenix & Scisson
Geology Support
Box 498, MS946
Mercury, NV 89023

T. G. Barbour
Science Applications Int'l. Corp.
1626 Cole Blvd.
Suite 270
Golden, CO 80401

G. R. Benson
Otto Torpedo Co.
P.O. Box 341
Duke Center, PA 16729

J. Butz
Denver Research Institute
University of Denver
P.O. Box 10127
Denver, CO 80210

E. Detournay
Dowell Schlumberger
P.O. Box 2710
Tulsa, OK 74101

R. Dynan
Center for Explosives Tech.
Campus Station
Socorro, NM 87801

G. J. Fillo
IRECO, Inc.
Eleventh Floor Crossroads Tower
Salt Lake City, UT 84144

W. L. Fourney
Mechanical Engr. Dept.
University of Maryland
College Park, MD 20742

G. B. Griswold
New Mexico Institute of Mining
and Technology
Campus Station
Socorro, NM 87801

D. G. Krugman
Radialfrac Services, Inc.
1805 Plato Road
Duncan, OK 73534-0988

T. Kurtz
Gas Research Institute
8600 West Bryn Mawr
Chicago, IL 60631

M. Lekas
Geokinetics, Inc.
391 Chipeta Way D-2
Salt Lake City, UT 84108

K. R. Mniszewski
UTRI
10 W. 35th Street
Chicago, IL 60616

H. H. Mohaupt
Servo-Dynamics, Inc.
1151 Estrella Drive
Santa Barbara, CA 93110

R. Nilson
S-Cubed
P.O. Box 1620
LaJolla, CA 92038

A. Rose
Servo-Dynamics, Inc.
Route 1, Box 132E
Rodd Field Industrial Park
Corpus Christi, TX 78415

J. F. Schatz
Science Applications Int'l. Corp.
10210 Campus Point Drive
San Diego, CA 92121

F. Stickland
HiTech Natural Res. Inc.
5635 S. Waterbury Way
Suite C202
Salt Lake City, UT 84121

C. Young
Sunburst Recovery, Inc.
P.O. Box 1173
Steamboat Springs, CO 80477

W. Stevenson
Servo-Dynamics, Inc.
200,215 - 10 Avenue S.W.
Calgary, Alberta, Canada T2P 0A4

1524	J. Jung
1524	L. M. Taylor
5160A	J. F. Cuderman (20)
6000	E. H. Beckner
6200	V. L. Dugan
6240	R. K. Traeger
6242	J. C. Dunn
6242	T. Y. Chu
6242	R. D. Jacobson
6250	B. W. Marshall
6253	D. A. Northrop (20)
6253	S. Finley
6253	J. C. Lorenz
6253	A. R. Sattler
6253	N. R. Warpinski
6314	D. A. Glowka
7116	S. R. Dolce
7131	B. G. Edwards
7131	J. S. Talbutt
7132	A. B. Church
7133	R. D. Statler
7133	J. D. Patrick (NTS)
3141	S. A. Landenberger (5)
3151	W. L. Garner (5)
3154-1	C. H. Dalin (28) for DOE/OSTI
8024	P. W. Dean

Org.	Bldg.	Name	Rec'd by	Org.	Bldg.	Name	Rec'd by

DO NOT MICROFILM
COVER

Sandia National Laboratories